DOE/MC/31178--5307
(DE97002047)

A Steerable/Distance Enhanced Penetrometer Delivery System Phase I

Topical Report

(August 1994 - August 1995)

by
Ali Amini
Joram Shenhar

August 1995

Work Performed Under Contract No.: DE-AR21-94MC31178

for

U.S. Department of Energy
Office of Environmental Management
Office of Technology Development
Washington, D.C.

U.S. Department of Energy
Office of Fossil Energy
Morgantown Energy Technology Center
Morgantown, West Virginia

by
UTD, Incorporated
Newington, Virginia

Disclaimer

DOE/MC/31178--5307
(DE97002047)

A Steerable/Distance Enhanced Penetrometer Delivery System Phase I

Topical Report

(August 1994 - August 1995)

by
Ali Amini
Joram Shenhar

August 1995

Work Performed Under Contract No.: DE-AR21-94MC31178

for

U.S. Department of Energy
Office of Environmental Management
Office of Technology Development
1000 Independence Avenue
Washington, D.C. 20585

U.S. Department of Energy
Office of Fossil Energy
Morgantown Energy Technology Center
P.O. Box 880
Morgantown, West Virginia 26507-0880

by
UTD, Incorporated
8560 Cinderbed Road
Suite 1300
Newington, Virginia 22122

ACKNOWLEDGMENT

The work presented in this report was sponsored by the Department Of Energy (DOE), Morgantown Energy Technology Center (MET), Office of Technology Development (OTD). Mr. Carl Roosmagi of DOE, METC, Laramie office was the contract monitor. Mr. Roosmagi's continued support is appreciated greatly. Mr. John Hall of the Ditch Witch of Georgia played a key role in successful field tests performed at his site in Atlanta, Georgia. Mr. David Timian and Mr. Wayne Russell of Applied Research Associates, Inc. provided access to the DOE SCAPS truck and assisted in POLO field tests. In addition to authors, the technical team working on this project consisted of Dr. Eugene Foster, Mr. Shervin Hojati, Mr. Kenneth Lum, Mr. Gregory Boyd, and Mr. Jim Laporte. The administrative staff at UTD who was instrumental in keeping track of contractual obligations, finances of the project, and production of timely reports included Mrs. Carol Horowitz, Mrs. Pam Burrowes, Mrs. Jane Whitten, and Ms. Maxine Emory.

TABLE OF CONTENTS

Page

TABLE OF CONTENTS (continued)

Page

LIST OF TABLES

Page

LIST OF FIGURES

LIST OF FIGURES (continued)

LIST OF FIGURES (continued)

Page

APPENDIX A

EXECUTIVE SUMMARY

Penetrometers play an important role in detection, mapping and remediation of underground contaminated sites. At present, penetrometer applications are restricted mainly to vertical pushes. This is due to a technology gap that exists in tracking and steering of the penetrometer tip. In the past five years UTD, Incorporated has worked to close this technology gap by developing an accurate and efficient position location system referred to as the POLO (POsition LOcation) device.

The prototype POLO device was developed under a PRDA contract sponsored by the Department Of Energy (DOE), Morgantown Energy Technology Center (METC), Office of Technology Development (OTD). At the completion of this contract, for the first time the penetrometer operator had the capability to know the position of the tip of the penetrometer in real-time. Building on this capability, UTD, Incorporated was awarded a follow-on three-phase contract under a Research Opportunity Announcement (ROA) program. The objectives of the new contract are to develop a steerable distance enhanced penetrometer delivery system, and to integrate POLO into a commercial penetrometer truck.

The Phase I work is the base year program and is comprised of sub-scale major sub-systems analysis and design of steering and vibratory penetrometer components. In addition, the Phase I work includes the integration of a POLO system into a commercial penetrometer truck. Through the analysis, design work and laboratory and field tests carried out in Phase I, the feasibility of a steerable penetrometer delivery system was demonstrated. In addition, it was shown that vibratory penetration increases depth of penetration by reducing the magnitude of the retarding forces on penetrometer rods. The prototype steering mechanism manufactured in Phase I is a semi-passive tip that can operate either in a straight ahead or in a curved mode based on rotation of penetrometer rods from the surface. Other components manufactured in Phase I include rod joints suitable for curved paths, joint locking mechanisms to resist steering torques, a commercial POLO initializer, and a commercial POLO unit.

Based on the results of Phase I work, it is recommended to continue the work and start Phase II work as scheduled. The work in Phases II and III include full-scale system design integration and field testing.

1.0 INTRODUCTION

1.1 Background

The characterization, monitoring, and remediation of many of the nation's highly contaminated sites are among the highest priorities of the Department Of Energy (DOE). In underground contaminated sites, detection and mapping of the plume of contamination and in-situ remediation are the first steps towards clean up. The needs for these steps include a depth capability ranging from tens of feet to between 100 to 200 feet, ability to go around underground obstacles with curvatures that do not damage downhole components, and downhole access for delivery of environmental sensors. In addition, in some instances it is necessary to use light weight equipment over underground storage tanks in order to avoid collapse of the tank. Baseline technologies of "aim and shoot" well drilling do not satisfy all of these needs, are not as efficient, and can further contaminate the site by bringing underground contaminants to the surface. As a result new technologies are needed to carry out underground site clean up more efficiently.

One system which has provided significant efficiency over baseline well drilling technology is the penetrometer. Using penetrometers, rods with an instrumented tip are pushed into the ground incrementally. In traditional penetrometer applications, the instrumentation package located at the tip measures soil resistance. However, for environmental monitoring purposes, an array of environmental sensors are packed inside the penetrometer rods for in-situ sampling and analysis, or for retrieval of laboratory samples. Examples of these sensors include soil samplers, the BAT groundwater monitoring sampling system, the PRT system for vapor sampling and the LIF system for in-situ detection of contaminants.

At present, penetrometer applications are restricted primarily to vertical pushes on the order of 100 to 200 feet. Because of their heavy weight, the use of penetrometer trucks over shallow buried storage tanks is restricted and costly. To close the technology gap in the use of penetrometers for environmental purposes, UTD took the first step by developing a new position location device for penetrometers referred to as POLO (short for POsition LOcator), which provides real-time position location without blocking downhole access for environmental sensors. The next step taken was the initiation of work to make penetrometers steerable and capable of greater penetration capabilities. The product of this work will be a relatively light weight steerable penetrometer that can provide greater penetration capability than traditional penetrometers of the same weight.

Competitive technologies for POLO include tilt sensors placed at the tip of penetrometers, accelerometers and magnetometers. Tilt sensors can only provide the tilt angle of the tip without providing information for real time tracking of the tip in three dimensions. Accelerometer arrangements that can provide data for real time tracking are expensive and block access to the tip of the penetrometer. Magnetometers are expensive and their capability is affected by magnetic anomalies.

A competitive technology for steerable penetrometer is directional drilling. Directional drills are used mostly for installation of underground pipes and utility cables. They use large amounts of water for drilling purposes and bring the cuttings to the surface. The problems with this technology are that the water used for drilling can spread the contamination further into the ground and the cuttings brought to the surface have to go through a clean up process.

The initial development of POLO was carried out through internal funds at UTD. Realizing the benefits of this new technology, DOE Morgantown Energy Technology Center (METC) funded the development of a prototype system under a PRDA contract. At the completion of the PRDA contract in September, 1994, for the first time the penetrometer operator had the capability to know the position of his sampling locations. Building upon this capability, DOE awarded UTD a new contract to develop a steerable distance enhanced penetrometer delivery system. In addition, in order to bring POLO into the commercial market in a timely fashion, the new contract was modified (in-scope modification) and new tasks were added to integrate a commercial POLO into a Site Characterization and Analysis Penetrometer System (SCAPS) truck. The new contract including its in-scope modification was awarded under a Research Opportunity Announcement (ROA) program and is comprised of a base program (Phase I) and two optional phases (Phases II and III).

1.2 Objectives

An objective of this research effort is to complete development of a steering capability and a vibratory thrusting capability for penetrometer delivery systems. Steering can allow for the controlled directional use of the penetrometer, and vibratory thrusting can provide greater depth penetration and improve the ability to penetrate harder materials. Another objective of the research effort is to integrate a commercial POLO into a SCAPS truck.

1.3 Scope of Work

The project consists of three phases. Phase I includes analysis, design, and laboratory experiments of the individual subsystems required to perform vibratory thrusting and steering of penetrometers. In addition, the work in Phase I includes design, assembly and integration of a commercial POLO system into a SCAPS truck.

Phase II work includes the integration of all steerable, navigational, and vibratory thrusting components and Phase III work includes field testing and demonstration of the full-scale integrated steerable/vibratory system.

The tasks in Phase I include:

Steerable and Vibratory Penetrometer Delivery System

Task 1.1	Environmental Work
Task 1.2	Steerable Wedge Design
Task 1.3	Survey of Vibratory Drives

Task 1.4	Joint Design
Task 1.5	Design of POLO Umbilical
Task 1.6	POLO Adaptation
Task 1.7	Theoretical Systems Analysis
Task 1.8	Experimental Evaluation of Components

Integration of a Commercial POLO system into a SCAPS Truck

Task 1.9	Design of Commercial POLO unit
Task 1.10	Data Acquisition Integration and Software Development
Task 1.11	Calibration and Field Tests

The Environmental Work task of the research effort included selection of uncontaminated sites for limited field tests as required. The selected sites were at the US Army Corps of Engineers facility, Ft. Belvoir, Virginia and Fredericksburg Sand and Gravel company in Fredericksburg, Virginia.

Details of research findings on Tasks 1.2 through 1.11 are reported in subsequent sections of this report. The findings reported are for the period of August, 1994 - August, 1995.

2.0 STEERING TIP ANALYSIS AND DESIGN

The field of environmental contamination assessment and cleanup capability created the need for advanced penetrometer systems. State-of-the-art penetrometer technology will enhance maneuverability and thrusting capability, opening the door to characterization and evaluation of critical environmental hazard areas such as contamination beneath buildings, pavements, storage tanks, buried pipelines, and landfills. Currently, penetrometer rods are passive devices used to deliver a set of sensors to a desired underground destination but with no ability of on-line trajectory alteration to correct for course alteration due to unforeseen obstacles. Upon successful completion of this contract initiative, which is the development of a steerable penetrometer, future penetrometer systems will include a steering mechanism, permitting maneuvering of the penetrometer tip. Due to this new driving strategy, penetrometer rods will be equipped with a directional tip, capable of generating transverse forces in order to achieve penetrometer steerability. State-of-the-art computerized control strategies may also be applied to the penetration process in order to enhance operation accuracy and human errors reduction. Prior to the development of such a system for commercial applications, a laboratory study was performed to identify system parameters, tool configuration, and operational procedures. The primary purpose of the study was to show that tip maneuver is possible and to determine procedure guidelines and operation boundaries. In the following paragraphs, a description of the steering methodology is provided. The description includes penetrometer rod and tip modeling, computer simulation of the penetration process in terms of tip trajectory, and sizing of the force-couple system associated with the penetration process. Laboratory test results validate the theoretical model, and test data are compared to simulation results. A few conceptual design ideas for possible commercial directional penetrometer tips are introduced at the end.

2.1 Analysis and Predictive Model

Steerability of a penetrometer may be defined as the ability to change the curvature of the rod and the orientation of its bending plane in real-time in order to achieve a prescribed penetration path. Steering can be activated by the application of a transverse force to the front end of the rod. Generation of such a force may be accomplished by a directional actuator in the form of a wedge or an oblique conical tip. The intensity of the force depends on the system parameters associated with the penetration process. Some of these parameters are related to the soil properties such as density, angle of internal friction, angle of friction between the soil and steel (skin friction), and point bearing capacity of the soil. Other system parameters are related to the rod material and diameters, the tip geometrical configuration, and penetration process dynamics. An analytical model has been employed for a preliminary study and simulation of the rod steering mechanism. For simplicity enhancement, the mathematical model used in this simulation represents a two-dimensional domain and is based on incremental insertion of a planar penetrometer rod equipped with a planar directional wedged tip.

The lateral deflection of each element was modeled as a beam in accordance with the "simple beam theory." The simulation generates the penetrometer rod trajectory and also computes the related force-couple history at the insertion point. A cantilever beam, shown in Figure 1, is selected

as the trajectory fundamental element, and the deflection and rotation of its free end are given in Equations 1 and 2, respectively.

$$y_i = \frac{Q_p \sin(\alpha-\delta) l_i^3}{3EI} + \frac{(q_p - q_0) l_i^4}{8EI} \operatorname{sgn}(\alpha-\delta) \tag{1}$$

$$\theta_i = \frac{Q_p \sin(\alpha-\delta) l_i^2}{2EI} + \frac{(q_p - q_0) l_i^3}{6EI} \operatorname{sgn}(\alpha-\delta) \tag{2}$$

where "sgn" represents the standard sign function defined as

$\alpha - \delta > 0$	$\operatorname{sgn}(\alpha - \delta)$	=	1
$\alpha - \delta = 0$	$\operatorname{sgn}(\alpha - \delta)$	=	0
$\alpha - \delta < 0$	$\operatorname{sgn}(\alpha - \delta)$	=	-1

In these expressions α is the wedge slope angle at the tip, δ is the friction angle between the soil and the beam material, Q_p is the tip point force, q_p and q_0 are the passive and at-rest distributed skin forces per unit length, respectively [1], l_i is the beam element length, E represents the modulus of elasticity of the penetrometer rod material, and I is the rod cross-sectional moment of inertia. The modeled trajectory is an evolution of sequential additions of one beam to another in a tail-to-head fashion and is depicted in Figure 1.

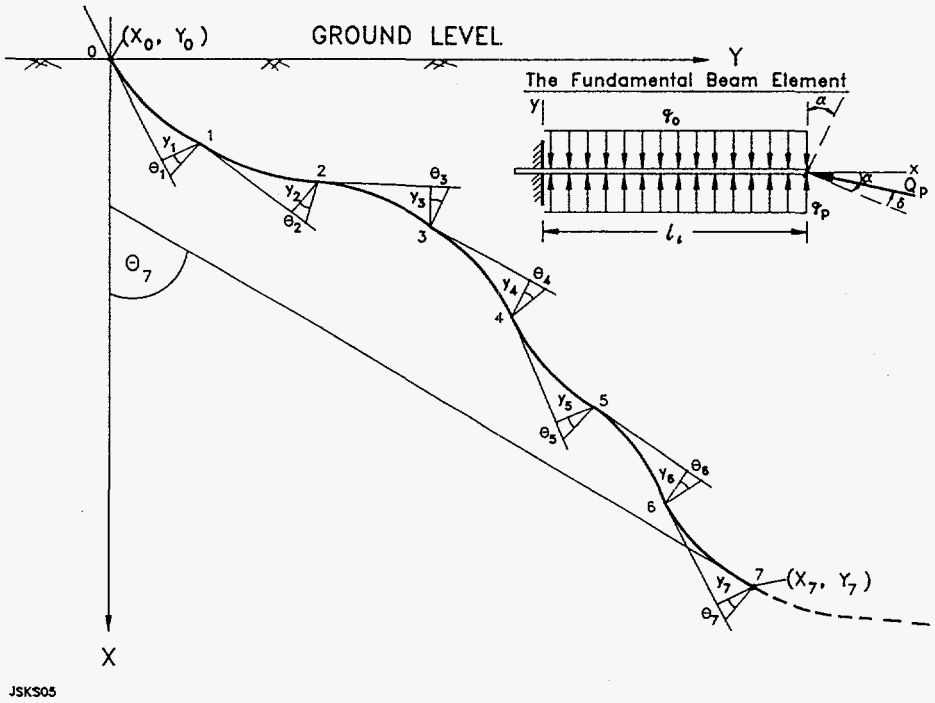

Figure 1. Penetrometer trajectory simulation model.

Let X,Y,Θ represent a triad of tip coordinates system and X_0,Y_0,Θ_0 their initial values, where X is the tip instantaneous depth, Y is its lateral displacement, and Θ is the tip instantaneous slope angle. The following spatial difference expressions may be derived for the triad, which may be cast in a compact form as follows:

$$X_i = X_{i-1} + l_i \cos\Theta_{i-1} - l_i \sin\Theta_{i-1} \tag{3}$$

$$Y_i = Y_{i-1} + l_i \sin\Theta_{i-1} + l_i \cos\Theta_{i-1} \tag{4}$$

$$\Theta_i = \Theta_{i-1} + \theta_i \tag{5}$$

I = 1, 2,...,n. The total length of the trajectory is $L = \sum_{i=1}^{n} l_i$

Applying soil mechanics principles, the distributed normal and skin friction forces were calculated along the penetrometer rod as well as the point force at the rod tip [1], [2]. The following parameters were selected for the simulation model

Soil Parameters:	
soil density	120 lb/ft^3
angle of soil internal friction	35°
angle of soil-steel surface friction	23°
bearing capacity parameter	170
Penetrometer rod parameters:	
outer diameter	1.75 in
inner diameter	1.00 in
modulus of elasticity	28*10^6 psi

The two-dimensional trajectory is generated by the deflected tip force. Figure 2 displays rod trajectories for various tip tilt angles.

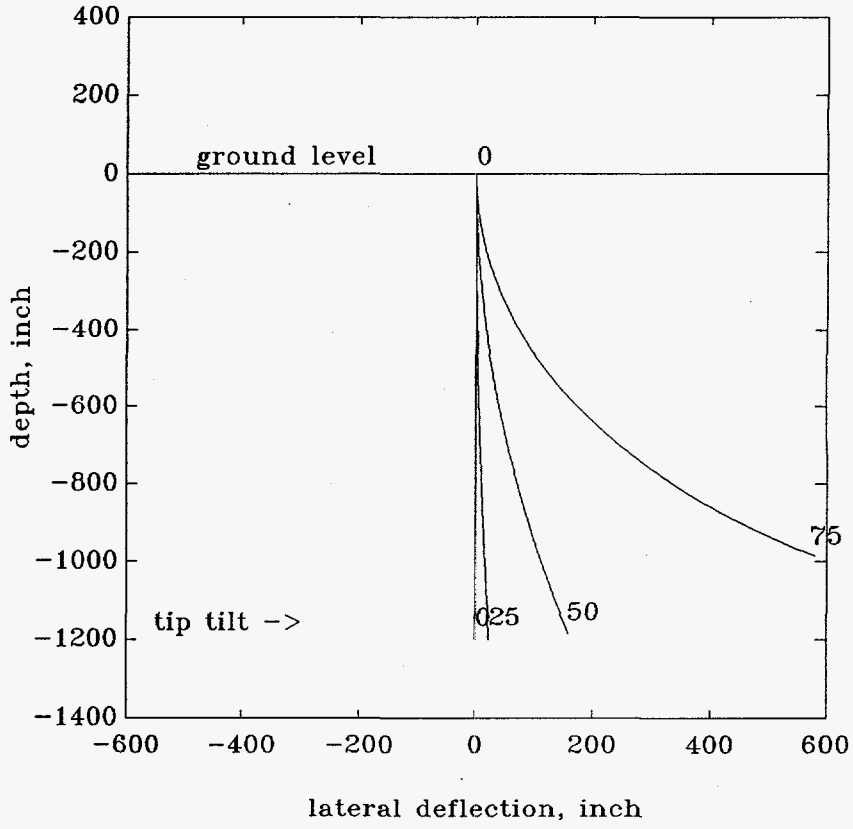

Figure 2. Penetrometer trajectories for various tip tilt angles.

In this study, the selected tip angle α is fixed in magnitude for a particular trajectory but its polarity may be changed from $+\alpha$ to $-\alpha$ due to a tip command. Typical penetration trajectories are displayed in Figures 3 and 4.

The rod in Figure 3 was pushed under a constant tip command $\alpha = 45°$. As a result, the rod deflected sideways as shown. The rod in Figure 4 was pushed under a variable tip command, half way with a tip tilt angle $\alpha = 45°$ and then, at a depth of 600 inches, the polarity was changed to $\alpha = -45°$ for an additional push of 600 inches. The shaded areas appearing in both figures represent the tip command polarity. Positive area represents tip angle driving the displacement to the right, and negative tip angle driving the displacement to the left. It is observed that though the two strokes were identical in length with tip tilt angle symmetrically inverted, due to the trajectory geometry, the tip sustained an unrecovered lateral displacement offset. Pushing of an additional half cycle with no change in the polarity will cause the trajectory to return to the zero deflection mark. Based on this "open-loop penetration philosophy", the penetrometer can be steered to a known location by changing the tip direction in response to the real-time tracking information provided by POLO.

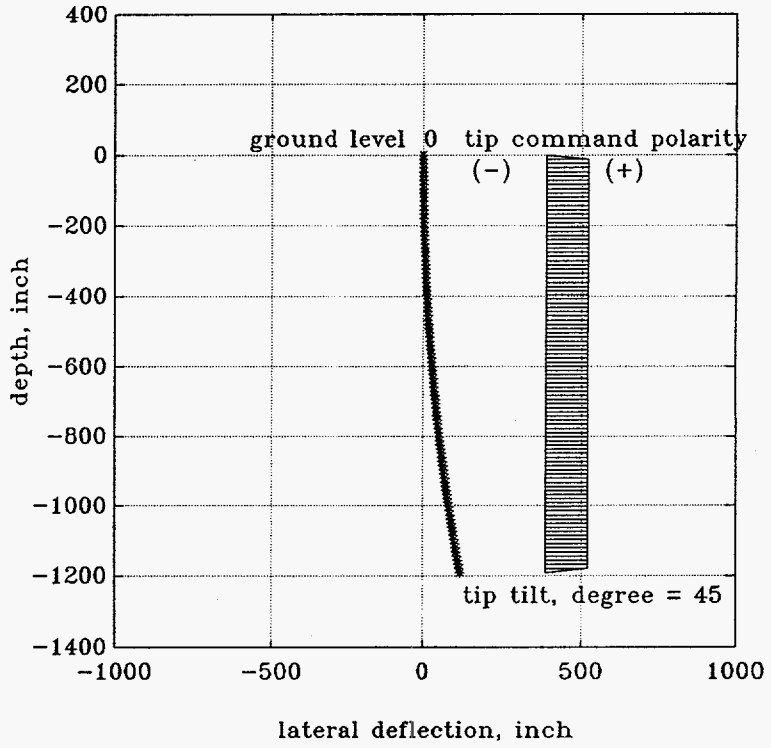

Figure 3. Penetrometer trajectory with constant tip command.

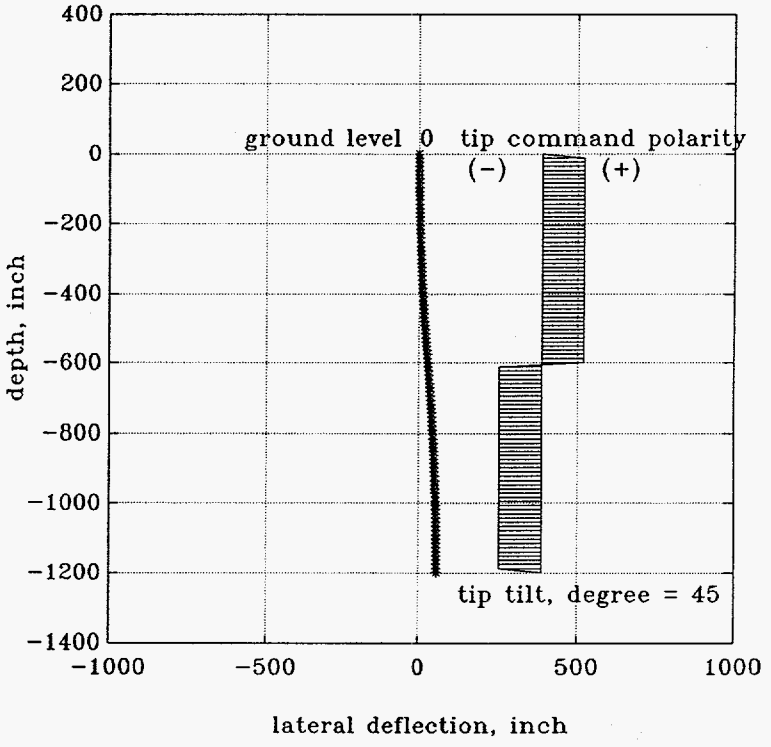

Figure 4. Penetrometer trajectory with variable tip command.

In addition to trajectory generation, the simulation also computes the force-couple system at the insertion point, namely, the system origin. Components of the force-couple are the reaction shear force perpendicular to the rod axis V, the normal "push" force along the rod axis of symmetry N, and the reaction couple M, as shown by the simulation model in Figure 5. The force-couple calculation for the entire insertion process provides the instantaneous reaction components as a function of the penetration depth that must be supported by the penetrometer insertion equipment. The simulated force-couple values are valid only at the insertion mode. The simulation does not reflect the reaction forces when the process is interrupted, since the tip point force Q_p and the skin friction f are then reduced to zero.

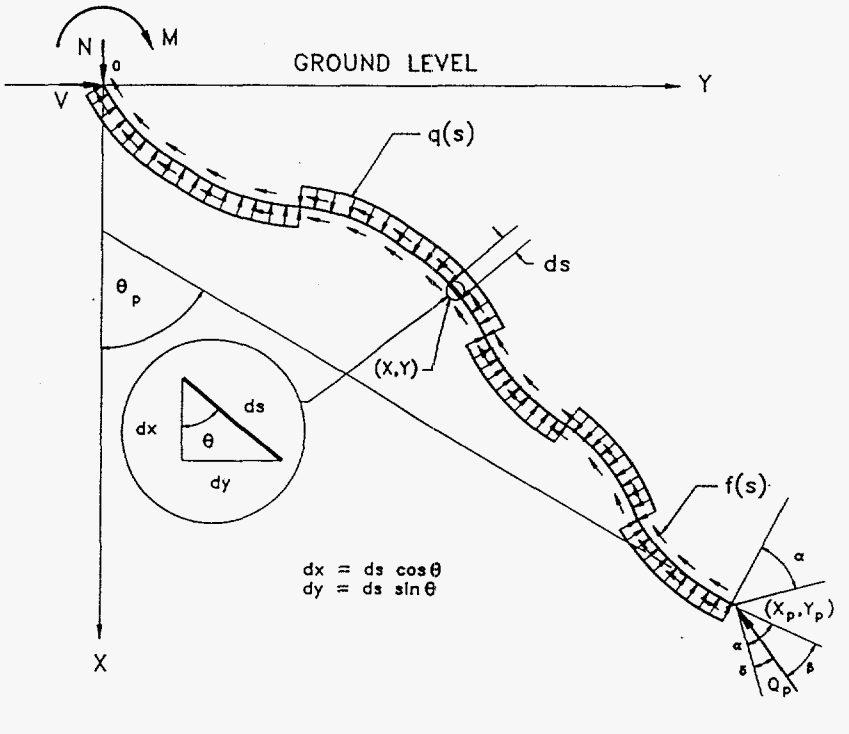

Figure 5. Penetrometer force-couple simulation model.

Figure 5 represents a free-body-diagram of the penetrometer rod in static equilibrium at time of insertion. Since the model represents a two-dimensional domain, the condition for equilibrium for the penetrometer rod may be described by three equations of equilibrium. Solution of this set of equations will yield the force-couple reaction components, V, N, and M, as follows:

$$\sum F_Y = 0; \quad \int_0^L q(s)\cos\Theta ds - \int_0^L f(s)\sin\Theta ds - Q_p \sin(\Theta_p - \beta) + V = 0 \qquad (6)$$

$$\sum F_X = 0; \quad -\int_0^L q(s)\sin\Theta ds - \int_0^L f(s)\cos\Theta ds - Q_p\cos(\Theta_p - \beta) + N = 0 \tag{7}$$

$$\sum M_0 = 0; \quad -\int_0^L q(s)(\cos\Theta X + \sin\Theta Y)ds + \int_0^L f(s)(\cos\Theta Y - \sin\Theta X)ds + Q_p\cos(\Theta_p - \beta)Y_p - Q_p\sin(\Theta_p - \beta)X_p - M = 0 \tag{8}$$

In these expressions X_p, Y_p, and ${}_p\Theta$ represent the triad of tip coordinates and rotation, respectively, while X, Y, and Θ represent the variable coordinates and rotation of any point on the trajectory between the origin and the rod tip, $q(s) = (q_p(s) - q_0(s))\ \mathrm{sgn}(\alpha - \delta)$, and $\beta = (|\alpha| - \delta)\ \mathrm{sgn}\ \alpha$.

2.2 Laboratory Steering Test

The model and methods previously described were used to conduct a set of laboratory experiments in order to test steerability capabilities of directional tips and also to validate the simulation model. Such validation will enhance confidence in the model and methods used, permitting the extrapolation of test and simulation results to real-time field work. Two phases of experiments were conducted. In the first, the test bed was constructed as a two-dimensional space to fit a two-dimensional rod and tip configuration. This reduced complexity arrangement allows comparison of test data to simulation results, as well as a preliminary validation of the steerability concept and capabilities. In the second phase of the experiment, the test bed was constructed as a three-dimensional space where a test rod simulating a penetrometer rod was tested for steerability. In both cases, the stiffness of the rod specimen was reduced so as to permit development of lateral displacements in the limited space of the laboratory environment. The test plan used for these experiments is presented in Appendix A.

Figure 6 depicts test results, where a rod with 5° wedge angle was pushed into wet sand under a constant tip command. The round labels seen on the front window indicate measured coordinates of the penetration trajectory. Comparison between simulation results and test data, shown in Figure 7, reveals good agreement. The departure of the test data from the simulation output toward the tip of the rod, shown in Figure 7, is mainly due to the proximity of the tip to the sandbox boundaries.

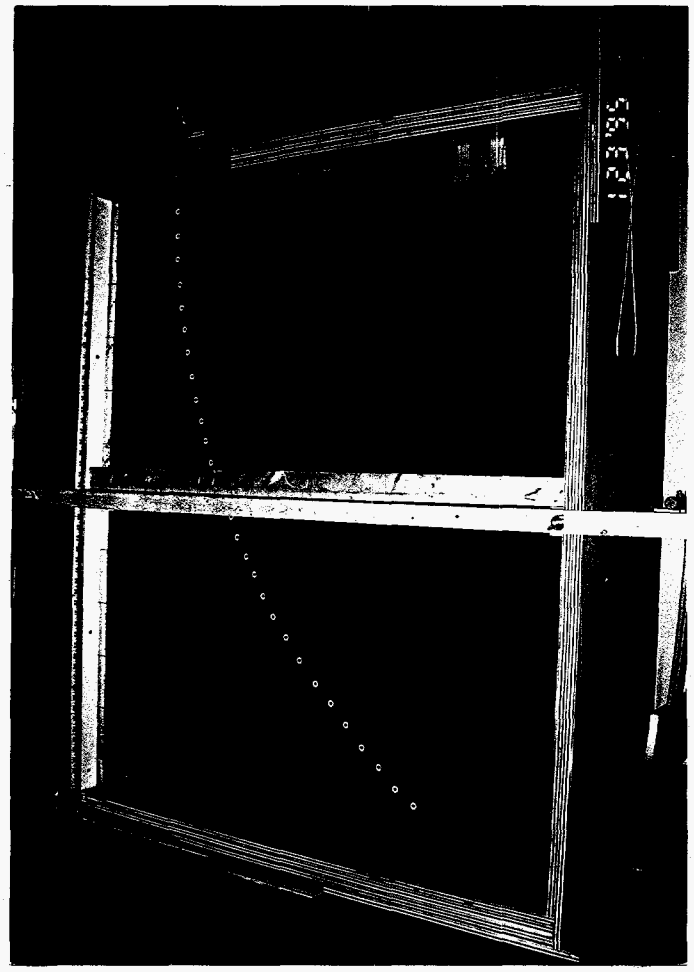

Figure 6. 5° wedge angle with constant tip command.

In another case, shown in Figure 8, the rod with 5° wedge angle was pushed into wet sand under a variable tip command. At about 18 inches deep, the rod was carefully pulled out all the way and then returned reversed, to reflect a change in tip command polarity from +5° to -5°. Also for this case, comparison between simulation results and test data, shown in Figure 9, reveals good agreement. Again, the departure of the test data from the simulation output toward the tip of the rod, shown in Figure 9, is mainly due to the proximity of the tip to the sandbox boundaries.

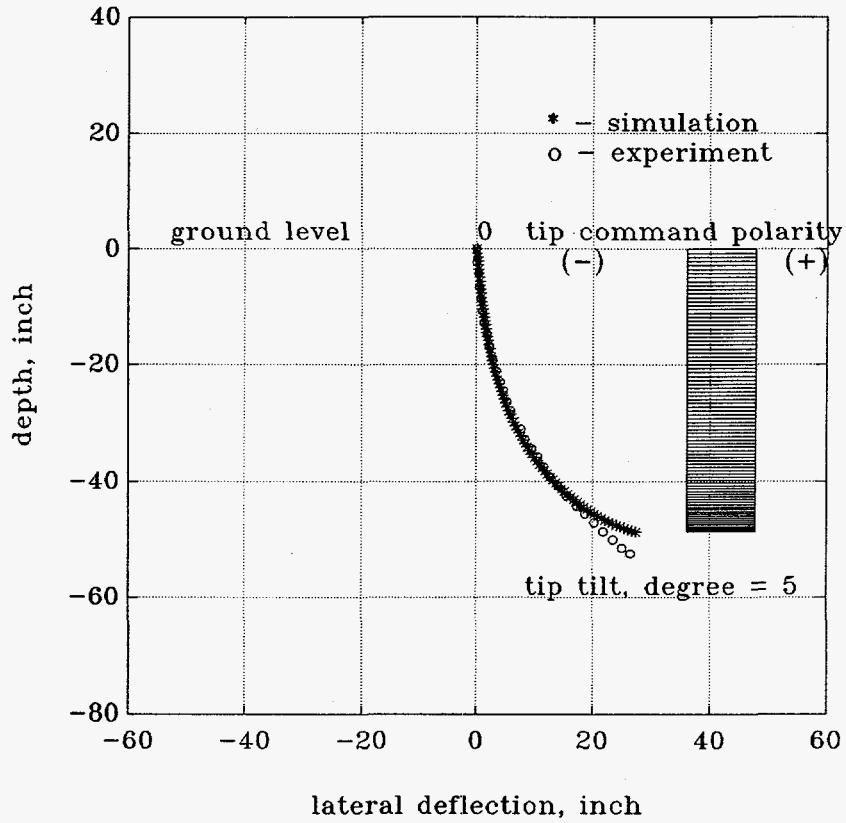

Figure 7. 5° wedge angle with constant tip command: trajectory - comparison between simulation results and test data.

Upon completion of the 2D tests, the sandbox was extended and tests were carried out in three dimensions using a cylindrical specimen with a 5° oblique cone as shown in Figure 10. Experimentally observed deflections are compared with simulation results in Figure 11. In Figure 12 the normal forces measured during the experiment are compared with those predicted by the simulation model.

The simulation study and laboratory test results provide an insight into the directional penetrometer technique and a preliminary parameter evaluation methodology. Test data collected at the sandbox experimental facility were used to establish initial guidelines for directional penetration. The results of the laboratory steering tests lead to two important conclusions. First, it is shown that it is possible to reverse the direction of travel of the penetrometer rod by changing the tilt angle of the tip. Second, the simulation model predicted deflections and force levels accurately. As a result, a very useful tool is now available for designing of the prototype and full-scale steering tips.

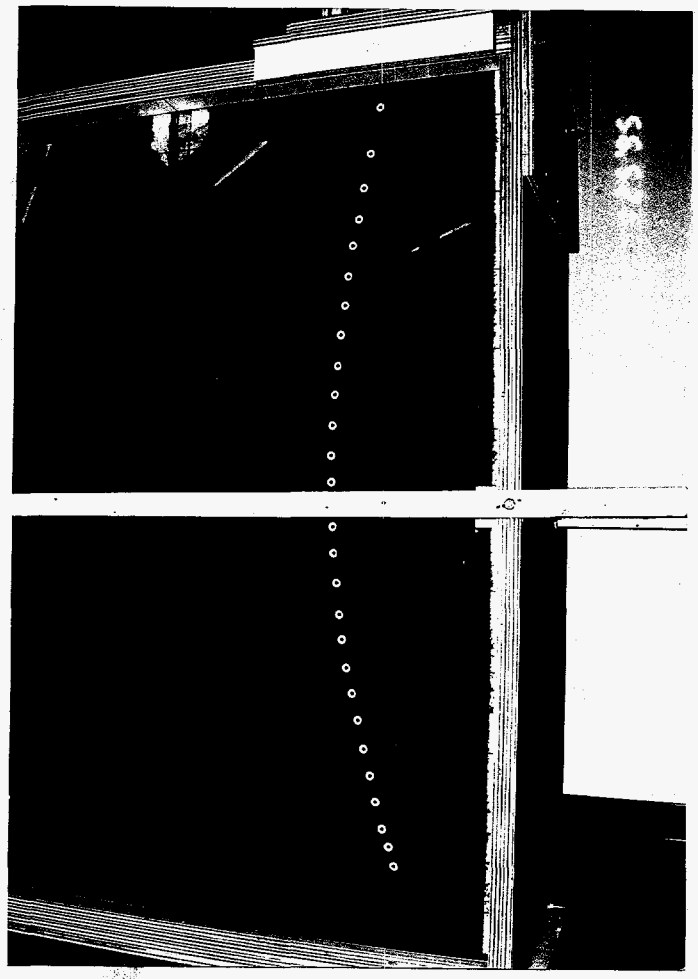

Figure 8. 5° wedge angle with variable tip command.

2.3 Steering Tip Design

Steerability is defined as the ability to change the curvature of a penetrometer rod and the orientation of its bending plane in real-time. Two main factors affect the ability to steer a penetrometer rod toward a prescribed target. One is the ability to generate a transverse bending force of a desirable magnitude at the penetrometer tip; the other is the ability to change its orientation with respect to the rod body so as to achieve tip spatial maneuverability. To this end, several design options were considered, some of which were of the passive tip configuration while others were associated with active tip mechanisms. All options considered for transverse force generation involved tips formed as a simple wedge or an oblique cone.

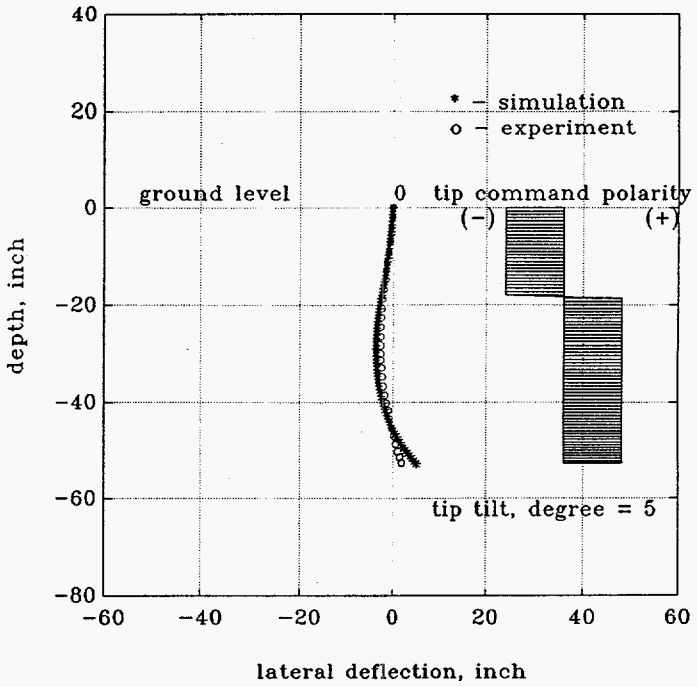

Figure 9. 5° wedge angle with variable tip command: trajectory - comparison between simulation results and test data.

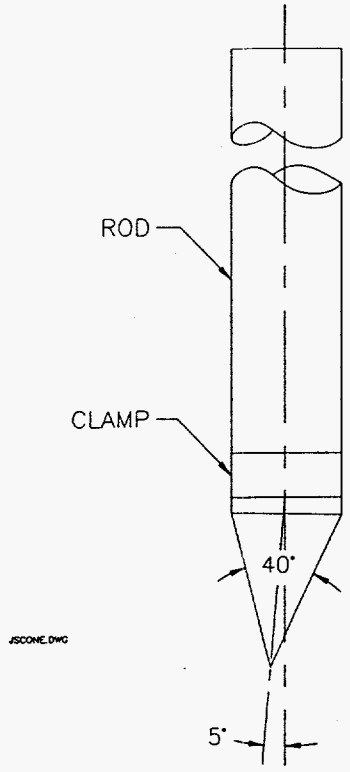

Figure 10. Cylindrical specimen with 5° oblique cone.

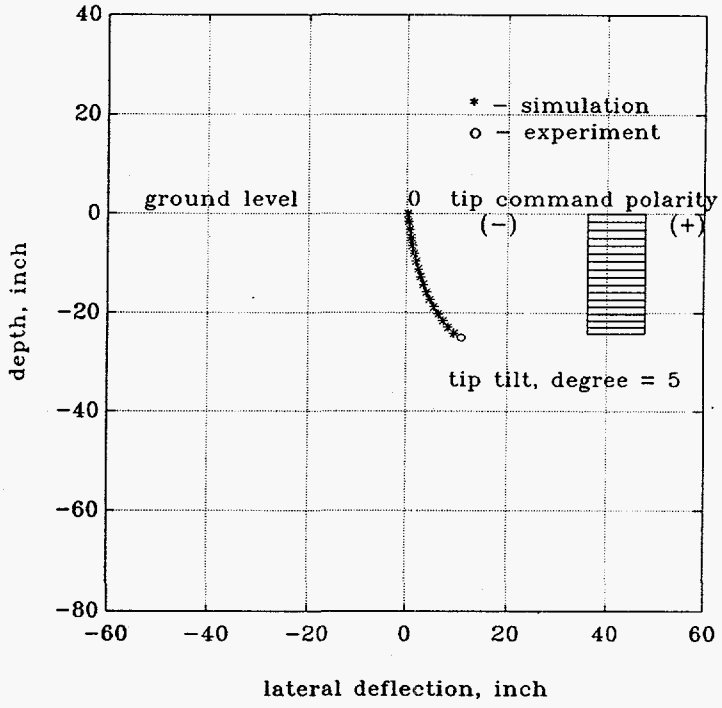

Figure 11. 5° cone angle: trajectory comparison between simulation results and test data.

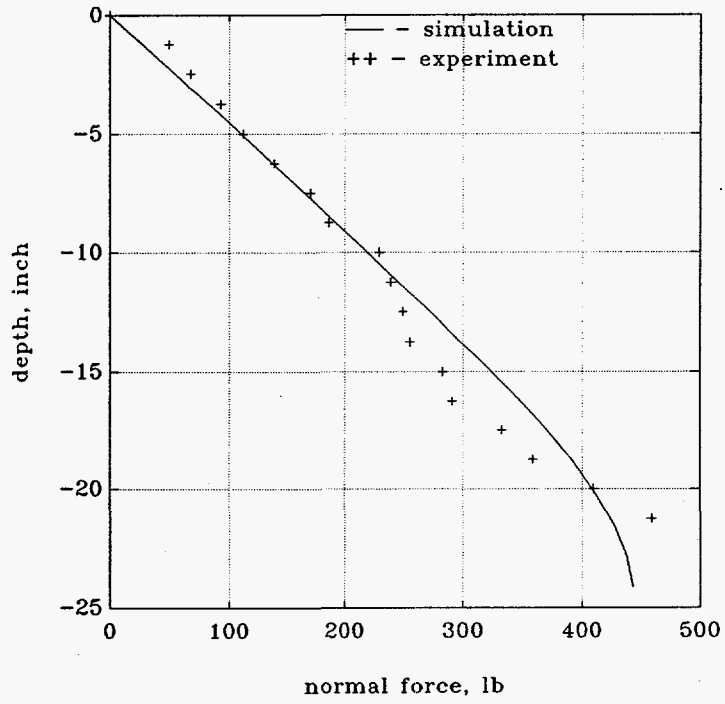

Figure 12. 5° cone angle: normal force comparison between simulation results and test data.

Using the passive tip approach, a fixed tip configuration is installed. Pushing of the penetrometer rod with such a tip generates rod deflection constantly. In order to reach a specified target, on-line tip position detection coupled with continuous reorientation of its transverse bending force is essential. Obviously, these activities must be commanded from the ground surface that calls for the application of an increasing continuous axial torque, to the entire penetrometer rod system. In long pushes the constant reorientation of the tip from the surface can slow down the penetration process considerably.

The active tip approach involves a mechanical tip installed at the rod front end that can be actuated to turn or change its position through signals sent from the surface. A tip for this purpose will have many mechanical parts and will require an umbilical for the actuation signals. Because of the vibratory nature of the penetration process, a mechanical tip with many parts is susceptible to breakdown and fatigue failure of components and connections. In addition, the actuation signal umbilical occupies a fairly large volume inside the penetrometer rods, leaving little or no space for the umbilicals of the environmental sensing instruments.

Realizing the disadvantages of the fully passive or fully active steering tips, it was decided to use a semi-passive tip developed by Foster-Miller Incorporated for ground piercing applications. The semi-passive tip shown in Figure 13 can be pushed into the ground either in a symmetrical configuration (as shown in the figure) or in an asymmetrical fashion as shown in Figure 14. The change from symmetrical to asymmetrical configuration is achieved by rotating the penetrometer rod by 180°. The stabilizer fins at the tip will keep the position of the tip locked until another 180° rotation is performed from the surface.

The advantages of the semi-passive tip are that the tip does not have to be reoriented continually from the surface, and it is made with very few mechanical parts, making it easy to use and control in the field. If an unexpected barrier is encountered the penetrometer tip can be drawn back and redirected to maneuver around the barrier. The turning radius limit of the prototype steerable tip manufactured in Phase 1 as discussed in Section 7.1 is between 90 to 115 feet. This is compatible with standard penetrometer joint limitations. For the full-scale system, the steerable tip may be deigned to provide a tighter turning radius compatible with the locking joints developed under this contract.

The simulation model described in Section 2.2 was used to determine the cone geometry and the attack angles that would result in radii of curvature larger than those causing rod failure. The prototype steering tip was manufactured and tested in the field. Details of these tests are presented in Section 7.

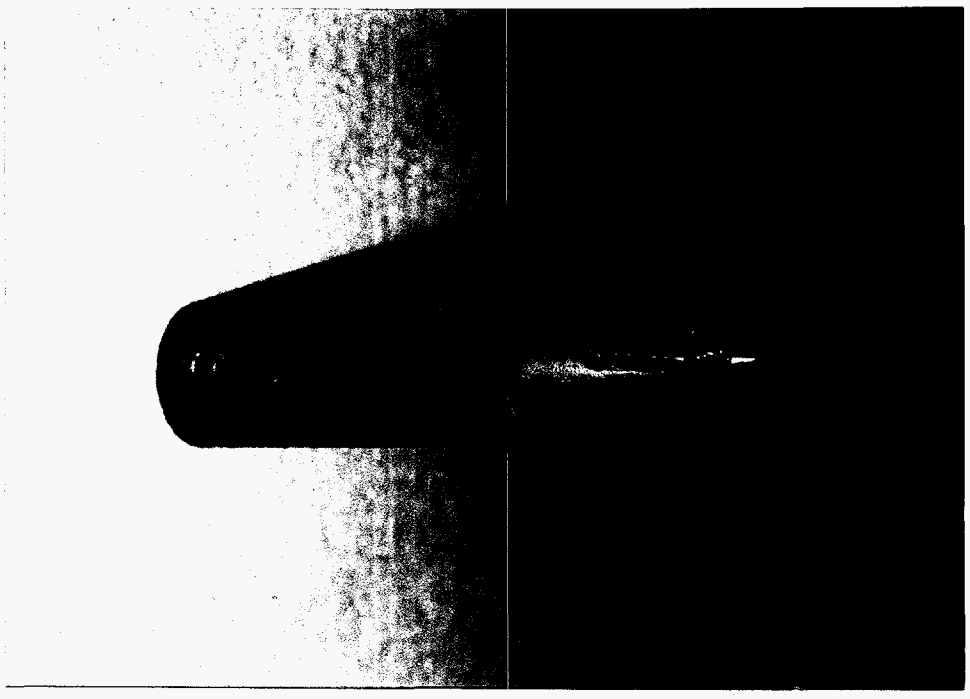

Figure 13. Semi-passive steering tip in a symmetrical configuration.

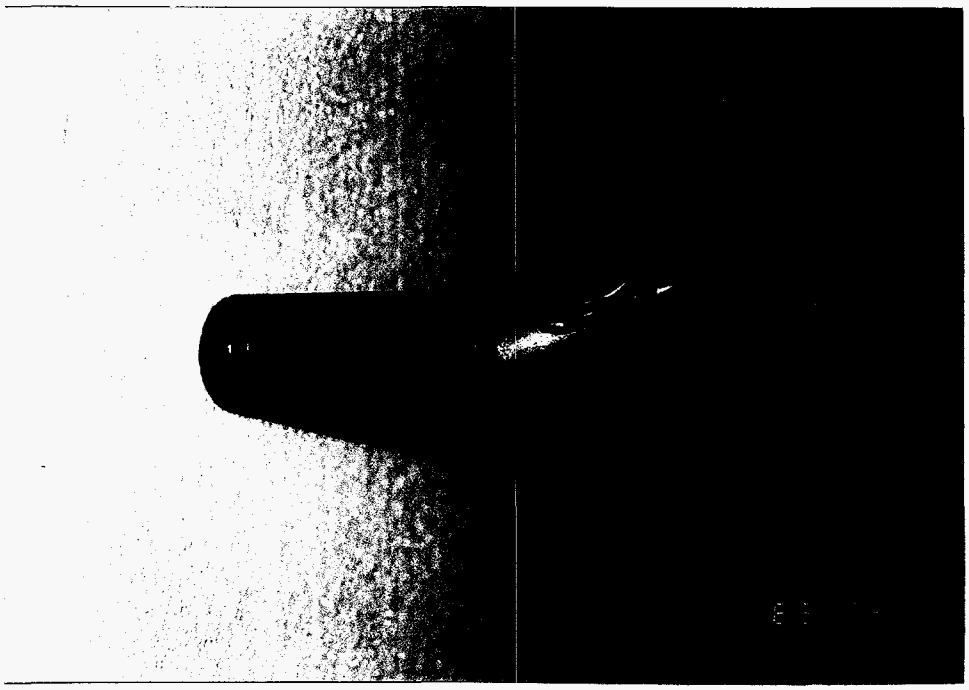

Figure 14. Semi-passive steering tip in an asymmetrical configuration.

3.0 SURVEY OF VIBRATORY DRIVES

Traditional penetrometer systems utilize hydraulic cylinders that apply a constant thrust to the rods. For this approach, the maximum thrust that can be applied to the rods is equal to the weight of the truck. As a result, heavy trucks are needed for long pushes or for penetration through hard materials. In an alternative approach, a lighter penetrometer rig may be used if part of the thrust is provided by vibratory means. If the frame of the penetrometer rig is isolated from vibrations, the dynamic load can be larger than the weight of the penetrometer rig resulting in a system that can push rods into the ground with a steady state force equal to the weight of the rig and a superimposed dynamic load which is a function of the frequency of vibrations.

Another benefit of vibratory pushing of the rods is the constant motion between the rods and the surrounding soil. This reduces the coefficient of friction between the rods and the soil form a static to a dynamic value, which in turn results in smaller thrust requirements.

In addition to vibratory loading, the steady state thrust capability of the penetrometer truck can be increased beyond the dead weight of the truck by anchoring the penetrometer rig to the ground. In this arrangement, the total pushing force is the weight of the truck plus the anchor capacity plus the dynamic load.

3.1 System Requirements

Several factors affect the performance of a vibratory penetrometer system. If the dynamic load is applied by a rotating unbalanced mass, its magnitude in the vertical direction is equal to:

$$F(t) = m_0 e \omega^2 \sin \omega t \qquad (9)$$

where m_0 = rotating mass,
e = radius to center of rotation
ω = angular velocity (circular frequency), and
t = time.

Based on Equation 9, the amplitude of the dynamic load ($m_0 e \omega^2$) varies with circular frequency ω. However, in order to benefit from resonance between the vibratory head and penetrometer rods and the resulting dynamic magnification, it is necessary to operate the system at a frequency close to the natural frequency of a penetrometer rod. As discussed in more detail in Section 6 the natural frequency of a penetrometer rod varies with the length of rod inserted into the ground. For example, for a 500" rod the natural frequency is 200 Hz, whereas for a 1200 inch rod the frequency drops to 82. Because of this variation, one of the system requirements is the ability to vary the operating frequency of the vibratory rig.

By reducing the frequency of vibrations as the length of the rods increases, the amplitude of the dynamic load ($m_0 e\omega^2$) decreases. Therefore, a balance has to be reached between operation close to natural frequency of the rods (lower frequencies at longer lengths) and a reduced dynamic load amplitude. The problem of reduction in force amplitude at lower frequencies can be overcome by increasing the vibratory mass at lower frequencies.

In addition to vibratory requirements, another important factor in selection of a penetrometer system is the required maximum thrust. Based on the simulation model of Section 2, using soil properties for a medium dense sand formation, the required thrust for pushing penetrometer rods 100 feet into the ground is 18,000 lbs. This is based on a static coefficient of friction of 0.36 between the rods and the sand. If this coefficient of friction is reduced by 25% due to vibratory loading, the required thrust drops to 13,500 lbs. A similar simulation in medium stiff clay results in 18,500 lbs of thrust using a static adhesion factor and 13,850 lbs if the adhesion factor is reduced by 25% due to vibrations.

A final consideration in selection of a penetrometer system is the ease of use and upgradability of the system. It may be more efficient to select a system that satisfies the minimum requirements and then upgrade it based on findings of performance tests on various components of the system. This consideration was taken into account in our selection.

3.2 Selected System Description

A search was performed to select an appropriate penetrometer delivery system. The systems considered included commercial sonic drilling rigs, commercial vibratory penetrometer trucks, and vibratory coring equipment. To enable an appropriate selection, the information related to operating envelopes, reliability, user friendliness, and adaptability were compared with the requirements of the system described in Section 3.1.

The selected vibratory system (shown in Figure 15) is called META-DRILL and is manufactured by MPI Drilling. An important feature of the META-DRILL is its modular construction. The system is made up of five modules that can be upgraded or replaced separately. These modules include the META-PRESS (mast module), vibratory drive, control module, hydraulic reservoir module, and power module. The following is a summary of the META-PRESS and the vibratory module capabilities:

<u>META-PRESS</u>

- 5 foot stroke
- up to 4 inch diameter rods
- bi-directional hydraulic
- down force 6,094 lbs (2770 kg) @2750 psi

VIBRATORY DRIVE

- hydraulic drive
- 7480 lbs (3400 kg) maximum centrifugal force at 200 Hz
- variable speed 10 to 200 Hz.

Figure 15. Breadboard META-DRILL vibratory penetrometer system.

4.0 JOINT DESIGN

The penetrometer joints which are commercially used today were designed to be used in penetrometer rods being inserted in straight trajectories. A typical penetrometer joint is shown in Figure 16. Under straight insertion conditions, the load is applied as axial compression which is carried by the shoulders of the mating rod sections. If the same joint is subjected to bending due to steering of the penetrometer tip or due to encounter with geologic anomalies, several weaknesses in the joint design may cause failure or permanent damage in the joint.

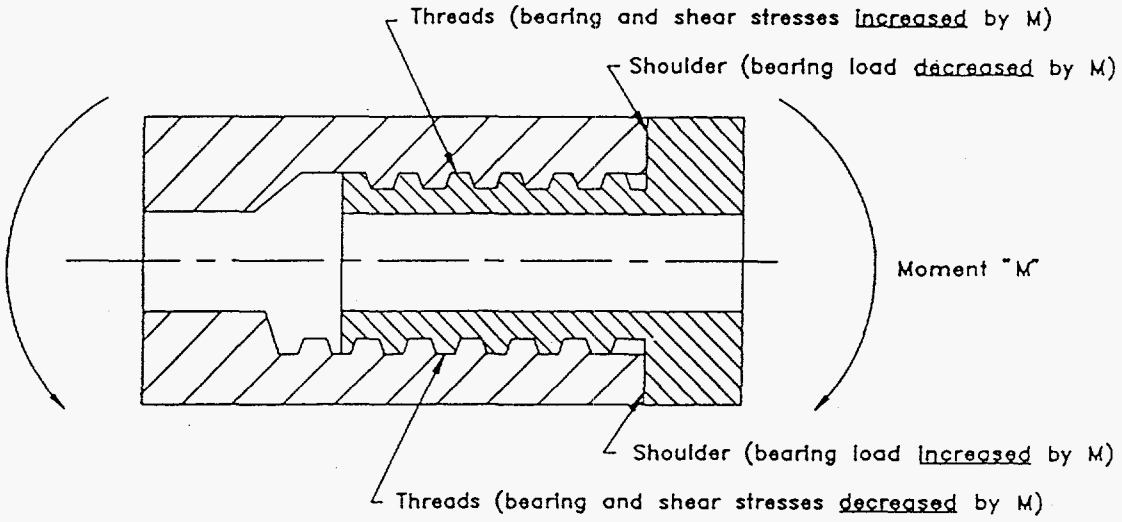

Figure 16. Off-the-shelf commercial penetrometer joint.

One of the weaknesses of a typical joint in bending is the shoulder contact. As shown in Figure 16, thread stresses are intensified in one region of the bend. In addition, the shoulder bearing load is decreased in the tensile region of the bend, and at small axial compressive loads this part of the shoulder may actually separate, resulting in a reduced section modulus. On the other hand, the opposite part of the shoulder will be subjected to increased bearing stresses which can permanently damage the joint.

Another problem with the use of commercial penetrometer joints in a steerable system is loosening of the joints under steering torques. This can happen when the rods are turned from the surface to steer the tip and the steering torque is applied in the opposite direction to that for tightening the joint. To overcome the loosening problem a locking mechanism has to be used with steerable joints.

4.1 Steerable Joint Design And Laboratory Testing

The joint developed for steering purposes is shown in Figure 17. This is an adaptation of an earlier UTD concept for a locking joint to be used with Steerable POLO. One of the main features of the joint is the absence of shoulders. Another feature of the joint is a straight section at the end of the male threads that guides the insertion of the male threads into female threads.

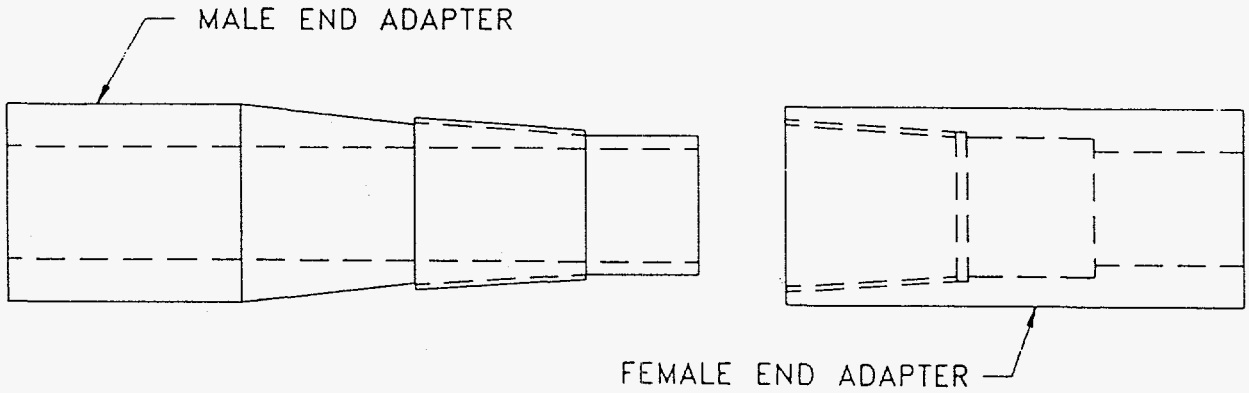

Figure 17. Steerable joint design.

The performance of the joint had to be verified before adding the locking mechanism. For this purpose, a set of new joints was machined and tested in a test frame built specifically for this purpose. The test frame shown in Figure 18 applies bending moments simultaneously with axial loads. The joint loadings can be varied independently.

Figure 19 is a summary of test results performed on four different rods made of the same material. In order to establish a baseline, one of the rods tested was jointless. The other three specimens were jointed rods, one using an off-the-shelf commercial penetrometer joint (shouldered joint), another using the new steerable joint design (shoulderless joint), and the third using the new steerable joint and a joint locking mechanism (locking joint). According to Figure 19, the jointless rod started yielding at a deflection of 0.21" which corresponds to a radius of curvature of 29'.

The curve for the shouldered joint had an initial dogleg at 0.07" deflection or 85' radius of curvature. This is believed to be due to separation of shoulders on the tension side and failure of the shoulder on the opposite side due to excessive compressive stresses. In fact, in practice it is common to keep the radius of curvature of commercial rods above 100' to avoid damage to the joints. Shoulder separation results in a change in the section modulus of the rod and the slope of the load-deflection curve as shown in Figure 19. Another observation related to the shouldered joint is the general yielding of the metal which starts at 0.17" of deflection or 35' radius of curvature.

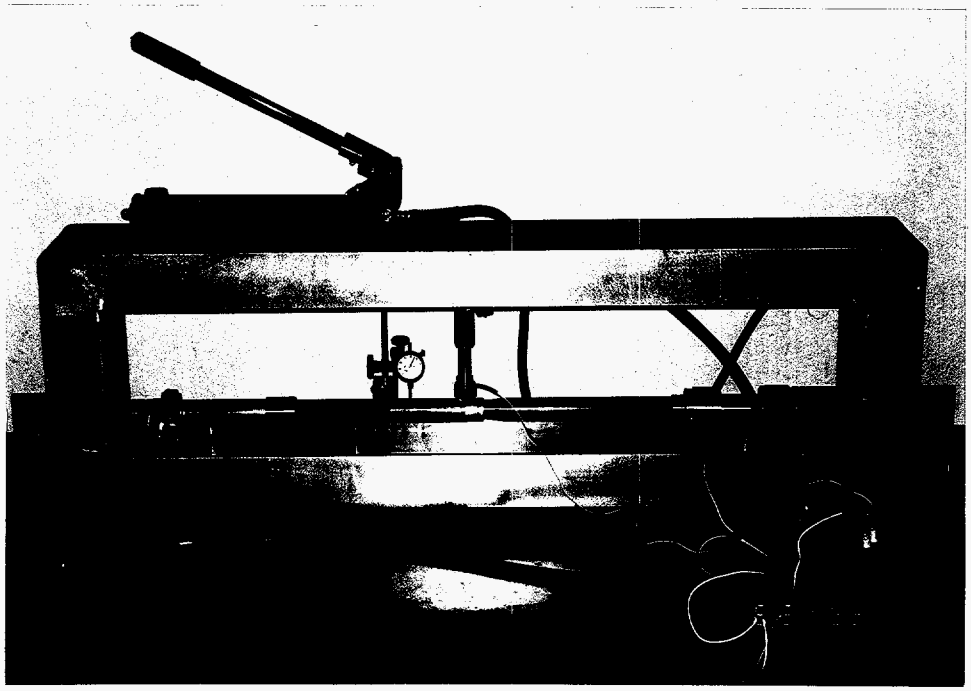

Figure 18. Test frame for laboratory testing of joints.

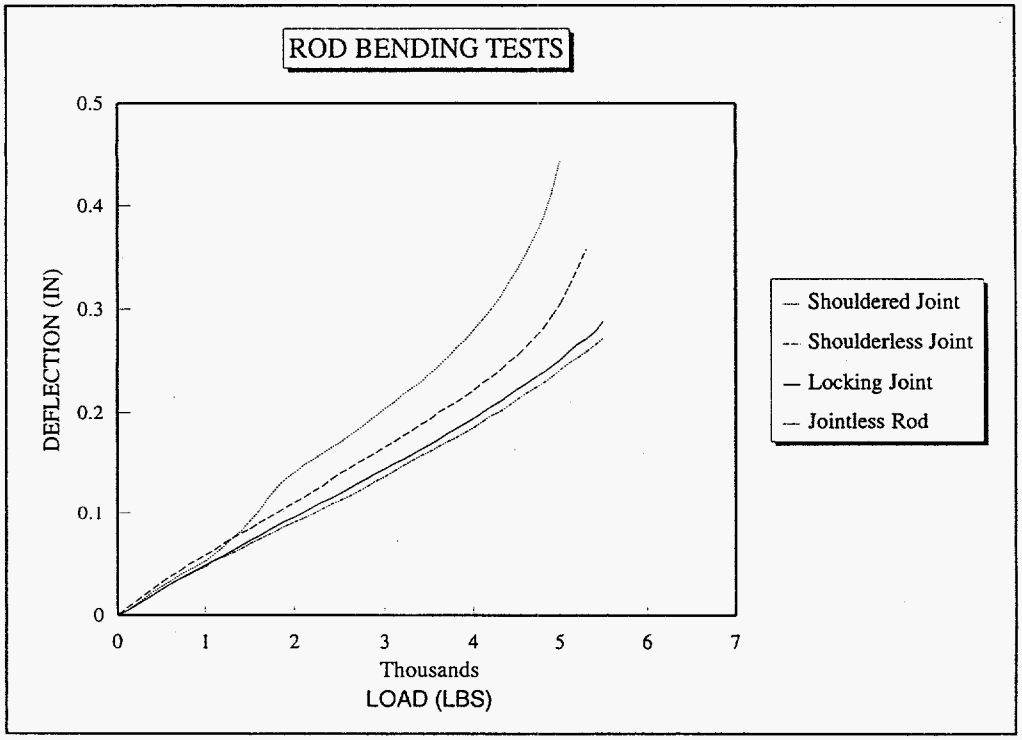

Figure 19. Results of laboratory tests on four rods.

The curve for the steerable joint (shoulderless) is very similar to that of the jointless rod except that the joint starts yielding at 0.19" of deflection or 31.5' radius of curvature. In contrast with the shouldered joint, the steerable joint does not go through a dogleg due to shoulder separation. From these results it was concluded that the performance of the steerable joint was superior and that it was suitable for use in steerable penetrometer applications. As a result, it was decided to continue with the joint design and refine it so that it could be locked against steering torques. The locking joint test results shown in Figure 19 are discussed in the following section.

4.2 Locking Joint Mechanism

An important design criterion for the steering joint is the ability to transmit torque without loosening the joint. To satisfy this requirement the original UTD locking joint incorporated a lock which was added to the configuration shown in Figure 17. The lock included a set of splines on the male end and a set of matching fingers at the female end as shown in Figure 20. The inner diameter of the female fingers is larger than the outer diameter of the male splines so that the joint can be tightened without interference between the male splines and female fingers. Upon tightening of the joint, the splines and the fingers are aligned and a shear plate ring that rides on the outer diameter of the male splines is inserted between the splines and fingers. The shear plate ring in effect locks the joint and prevents threads from opening under the steering torque.

Bending test results on the steerable joint equipped with the locking mechanism of Figure 20 are shown in Figure 19, (Locking Joint). The curve for the locking joint has for all practical purposes approached that of the jointless rod, implying a near perfect joint. The results of performance tests, including a torque test and a field test on the locking joint, are presented in Section 7.0.

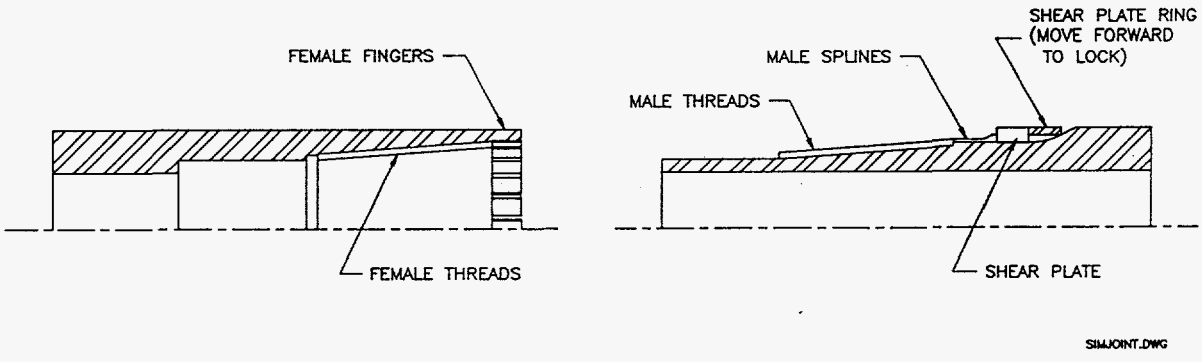

Figure 20. Locking joint mechanism.

5.0 POLO ADAPTATION AND POLO UMBILICAL

POLO is the position location system developed by UTD for use in penetrometers. Figure 21 is a cutaway schematic that shows the POLO module that was developed for field testing and demonstration under a previous PRDA contract. POLO is essentially a bending transducer rod that replaces the penetrometer rod just behind the tip. In the original design three sets of strain gages, equally spaced along an inner core, monitored bend orientation and intensity. The POLO tracking program uses the bend orientation and intensity at the end of each penetration cycle to update the location of the tip of the penetrometer.

As shown in Figure 21, an umbilical (bundled signal wires) made up of 24 wires connected the strain gages to the surface computer. To protect the strain gages from the harsh underground environment, the module was installed inside a shield with two epoxied end adapters for connection to penetrometer rods.

The POLO design shown in Figure 21 accomplished its mission of system demonstration successfully when it was used under the traditional pseudo-static penetration conditions. A different environment is encountered when penetrometer rods are steered around tight radii using vibratory means. As a result, the POLO design had to be refined for adaptation to the new conditions.

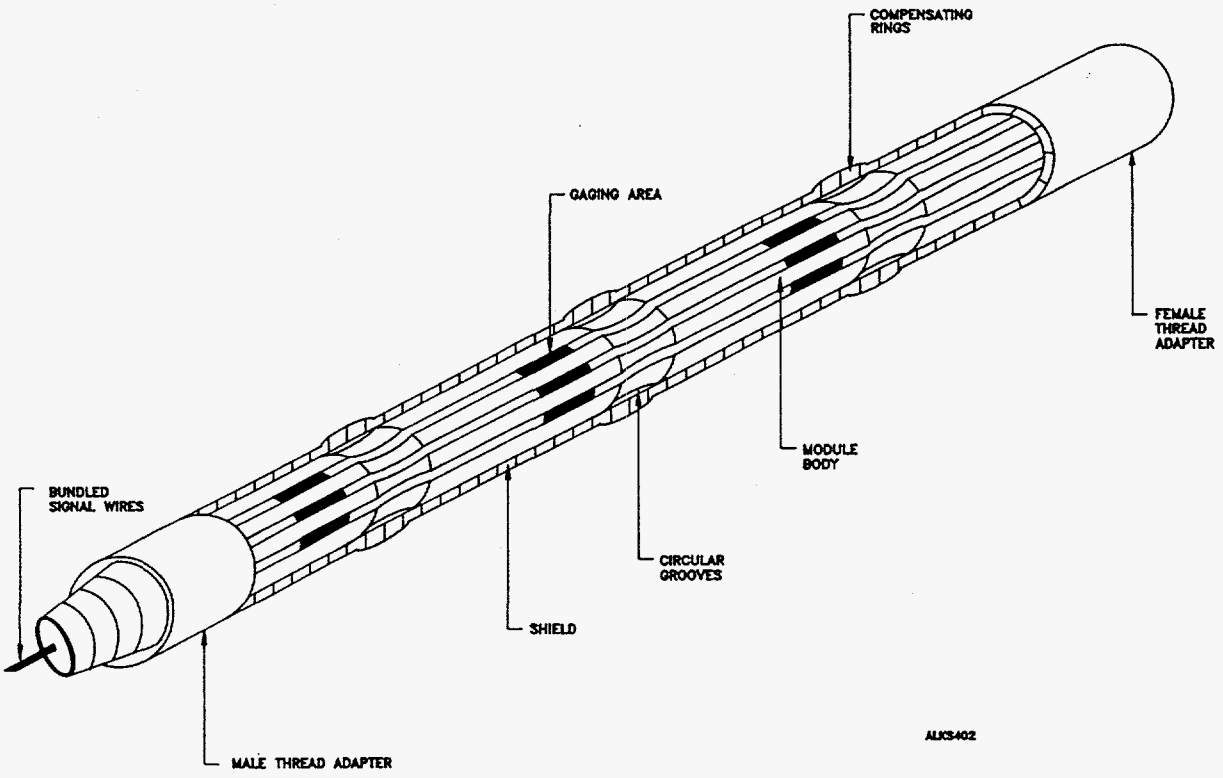

Figure 21. Original full-scale POLO module.

5.1 Reconfigured Strain Gages

Three sets of strain gages (stations) were used in the POLO device shown in Figure 21. At each gage station two full bridges were completed as shown in Figure 22a. In this configuration, strain readings from the two bridges are 90° apart.

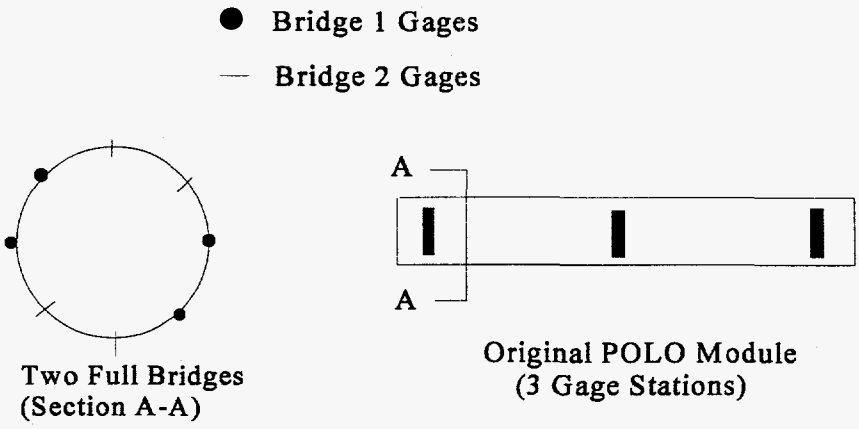

22a - Original POLO Strain Gage Configuration

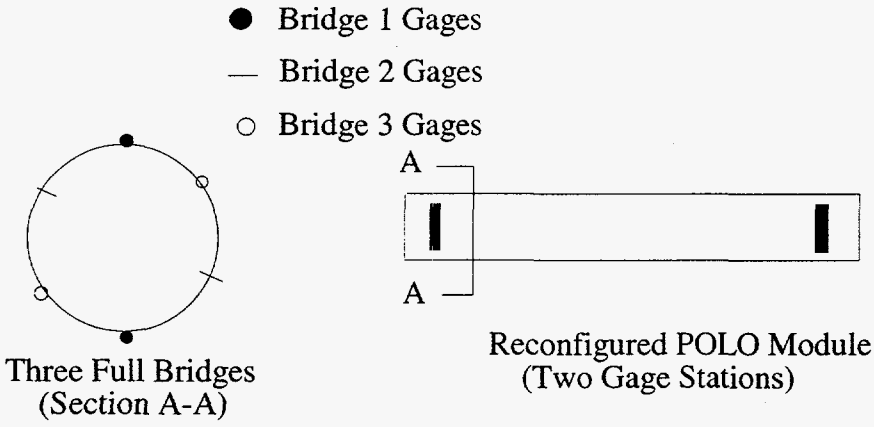

22b - Reconfigured POLO Strain Gage Configuration

Figure 22. Strain gage configurations.

When a pipe is subjected to bending, the strain around the circumference of any plane perpendicular to the longitudinal axis of the pipe varies sinusoidally as shown in Figure 23. The maximum bending strain and bend plane orientation with respect to a reference gage are two important parameters that are used by the POLO tracking program. These parameters can be back calculated from any two strain readings around the periphery of the pipe. For the bridge

configuration of Figure 22a, if one of the strain readings is made close to where the maximum strain occurs, the other reading will occur where the strain is close to zero as shown in the first half of the sine curve of Figure 23. In this case slight deviations in strain readings will cause large errors in back calculating the orientation of the bend plane. This is of special importance in steerable penetrometer applications where penetrometer rods are rotated from the surface.

To overcome the problem associated with two bridges 90° apart, the strain gages were reconfigured so that at each gage station three full bridges 60° apart were installed as shown in Figure 22b. In this configuration, if one of the bridges is located where the maximum strain occurs (shown in the second half of the sine curve of Figure 23) one can use the other two bridge readings to calculate the maximum strain and bend orientation. In order to keep the total number of strain gage bridges to six the middle gage station was eliminated in the reconfigured version. This was evaluated analytically and experimentally and shown not to have an adverse effect on POLO accuracy.

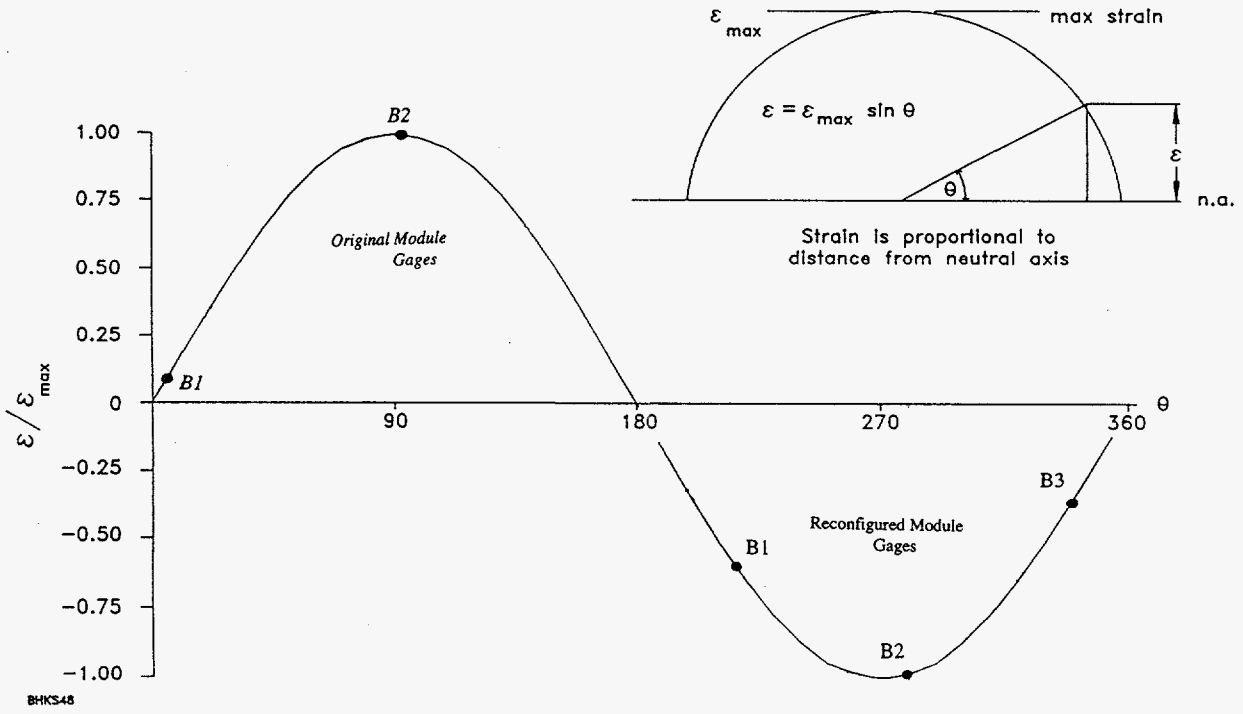

Figure 23. Strain variation around module perimeter.

5.2 Reconfigured Module Body

There were two major drawbacks associated with the original POLO module design in vibratory and steering applications. First, the epoxied end adapters of the shield were susceptible to breaking under constant vibrations and the bends associated with steering. A second drawback was the use of shouldered joints between the end adapters and the shield. As shown in Section 4, shouldered joints are susceptible to failure under large bends. To overcome these

problems with the original POLO design, the lead end adapter is thread connected to the shield and the lag end adapter welded to the shield. In addition, shouldered contacts at all the joints are replaced with shoulderless contacts.

5.3 Design of POLO Umbilical

The original POLO system utilized a portable data acquisition (DAQ) package at the surface. For this purpose a POLO umbilical made up of 24 wires connected the strain gages to the surface system. An umbilical with 24 wires is susceptible to damage and breaking in a vibratory environment. To reduce the risk of damage, the system was designed to use a down-hole DAQ system developed by UTD under an Internal Research and Development (IR&D) program.

The UTD DAQ system shown in Figure 24 fits inside the POLO module and occupies less than half of the available space. This leaves more than half of the space available inside penetrometer rods for other umbilicals used for environmental sampling. The system performs the following operations:

- preamplifies and filters each bridge readout,
- multiplexes the readouts from the six bridges,
- amplifies the multiplexed signals,
- digitizes signals,
- transmits digital signals to the surface processor,
- surface processor captures signals, formats data and transfers data to the computer.

The digitized signal is transmitted to the surface computer through only two wires. The same two wires are used for powering the device down hole. For the vibratory and steerable penetrometer applications it was decided to eliminate the POLO umbilical by using the penetrometer rods as one of the conductors and quick-connects at the ends of each penetrometer rod that provide connections for the second conductor wire as shown in Figure 25. The quick-connects at each end of a rod are connected to each other by a wire that is spot epoxied to the inner periphery of the rod. The quick-connects provide automatic and safe connection for the conductor wire at each joint as the joint is tightened by the penetrometer operator.

In order to determine the feasibility of using penetrometer rods and quick-connects to carry the down-hole signals to the surface, a set of laboratory tests was carried out. In these tests mock ups of the quick-connects were manufactured for 14 pipes. Then, a signal typical of that generated by the UTD down-hole system was sent from one end of the string of rods and monitored at the other end of the rods. As shown in Figure 26, the shape of the pulse remained practically unchanged. During these tests the pipes were bent on purpose and were subjected to vibrations and shock loading in order to simulate field conditions.

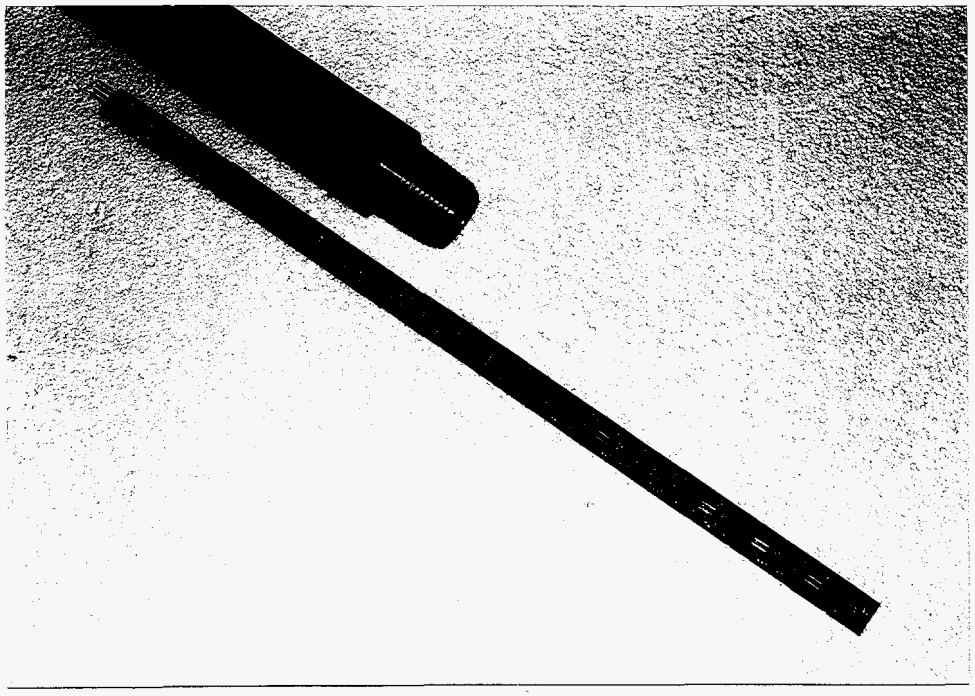

Figure 24. UTD down-hole DAQ system.

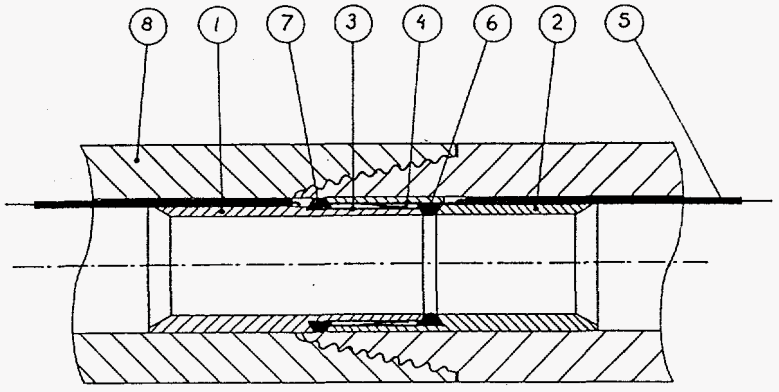

1. Lexan Connector Housing - Male
2. Lexan Connector Housing - Female
3. Copper Conductive Surface
4. Beryllium Copper Contact Blade
5. Lead-Wire
6. O-Ring Seal-Inner
7. O-Ring Seal-Outer
8. Penetrometer Rod

Figure 25. Schematics of the quick-connect concept.

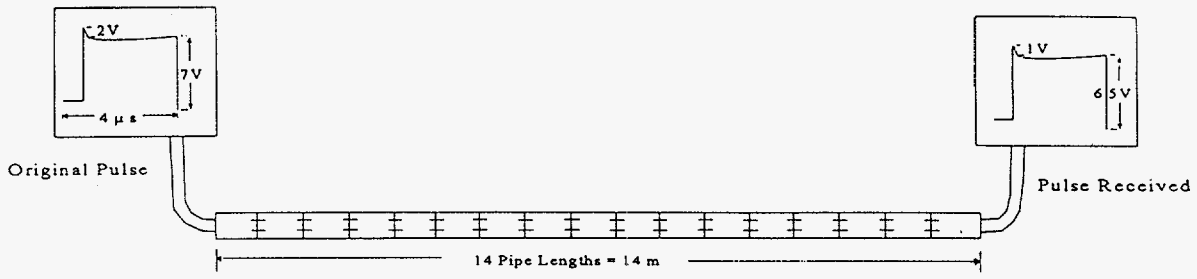

Figure 26. Laboratory test results for signal integrity.

6.0 THEORETICAL SYSTEMS ANALYSIS

Vibrations and steering related bends have adverse effects on performance of the penetrometer system. The laboratory and limited field tests performed on each component of the system verify performance over a limited range of vibrations and bends. A theoretical analysis of the overall system augments the experimental results and provides a useful tool to establish the operational envelopes of the system. An area of interest in a vibratory steerable penetrometer system is the vibrational modes of the system and their effects on stress distribution in the rods and joints.

6.1 The Resonance Penetrometer Method

Inserting penetrometer rods into the ground by vibratory means can be accomplished more efficiently if the applied excitations have a frequency as close as possible to the rods' natural frequency. Referring to this method as the Resonant Penetrometer Method (RPM), when any of the excitation frequencies coincides with one of the natural frequencies of the system, theoretically the response becomes infinite. This phenomenon known as the "resonance condition" is characterized by violent vibrations so as to facilitate quick and easy penetration of the rod into the ground. In the following discussion, elements of modal analysis, natural modes of vibration, and the response of a rod in longitudinal motion to a sinusoidal excitation, are discussed in order to provide insight into the RPM and quantitative tools for design.

6.1.1 Natural Modes Of Vibration Of A Rod In Longitudinal Motion

A description of a rod, free at both ends, in longitudinal motion is provided in Figure 27. EA(x) denotes the rod stiffness, m(x) is the mass per unit length, and u(x,t) represents the longitudinal displacement. For the free vibration analysis there are no external forces present.

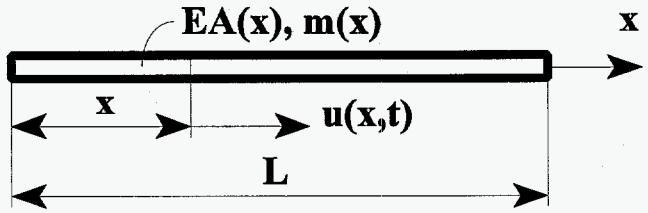

Figure 27. A thin rod, free at both ends, in longitudinal motion.

The differential equation and the associated boundary conditions for the longitudinal motion of a thin rod, free at both ends, may be derived using Hamilton's principle [3].

$$\frac{\partial}{\partial x}\left[EA(x)\frac{\partial u(x,t)}{\partial x}\right] = m(x)\frac{\partial^2 u(x,t)}{\partial t^2}\ , \qquad \left(EA(x)\frac{\partial u(x,t)}{\partial x}\right)\delta u\ |_0^L = 0 \tag{10}$$

The method of separation of variables is used to obtain the natural modes of vibration.

$$u(x,t) = U(x)\,f(t) \tag{11}$$

$U(x)$ is a spatial displacement function and $f(t)$ is a harmonic function of time with angular frequency ω. Substitution of (11) into (10) and considering a uniform rod for which the distributed mass m and the rod stiffness EA are constants, Equation (10) may be reduced to the simplified differential equation

$$\frac{d^2U(x)}{dx^2} + \beta^2 U(x) = 0\ , \qquad \beta^2 = \omega^2\frac{m}{EA} \tag{12}$$

and the associated boundary conditions representing the free-at-both-ends rod are

$$\frac{dU(x)}{dx}\ |_{x=0} = 0\ , \qquad \frac{dU(x)}{dx}\ |_{x=L} = 0 \tag{13}$$

Substitution of the general solution $U(x) = C_1 \sin\beta x + C_2 \cos\beta x$, together with the boundary conditions (13) into Equation (12), yields an expression for the natural frequencies and the corresponding normalized natural modes of vibration, respectively:

$$\omega_r = r\pi\sqrt{\frac{EA}{mL^2}}\ , \qquad r = 0,1,2,... \tag{14}$$

$$U_0(x) = \frac{1}{\sqrt{mL}}, \qquad U_r(x) = \sqrt{\frac{2}{mL}}\cos r\pi\frac{x}{L}, \qquad r = 1,2,... \tag{15}$$

The first equation in (15) represents the rigid body mode while the second represents the infinite number of elastic modes. Figure 28 displays the rigid body mode and the lowest three elastic modes of vibration for a 100 ft long steel tube, free at both ends, having the following parameters:

outer diameter	1.75 in
inner diameter	1.00 in
modulus of elasticity	$28*10^6$ psi
mass per unit length	$1.18*10^{-3}$ lb sec^2 in^{-2}

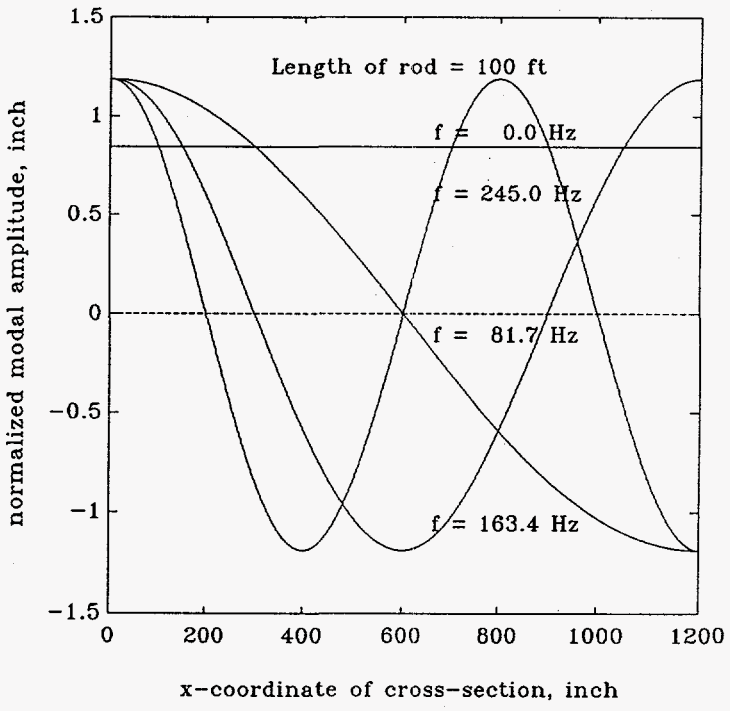

Figure 28. Rigid body and elastic modes of vibration of a rod free at both ends.

According to Equation (14), the natural frequency of the rod is inversely proportional to its length. Employing the Resonance Penetrometer Method, it is important to operate the vibratory head of the pushing machine at a frequency as close to the natural frequency as possible. To meet this goal, the excitation frequency must be lowered as the push process proceeds and the rod becomes longer. Figure 29 displays the natural frequency variation of the lowest mode of vibration as a function of the rod length.

Clearly, a rod pushing machine that operates in the range of 0 to 300 Hz will be less effective when RPM is applied to rods below 300 inch of length. In order to extend the range of operation so as to accommodate shorter rods, the natural frequency of a rod may be lowered somewhat by adding to the rod an auxiliary mass near its upper end above the ground. However, in the practical case this may not be necessary, since a static push is sufficient to advance the penetrometer in most soil types when the rod length is 300 inches (25 feet) or less.

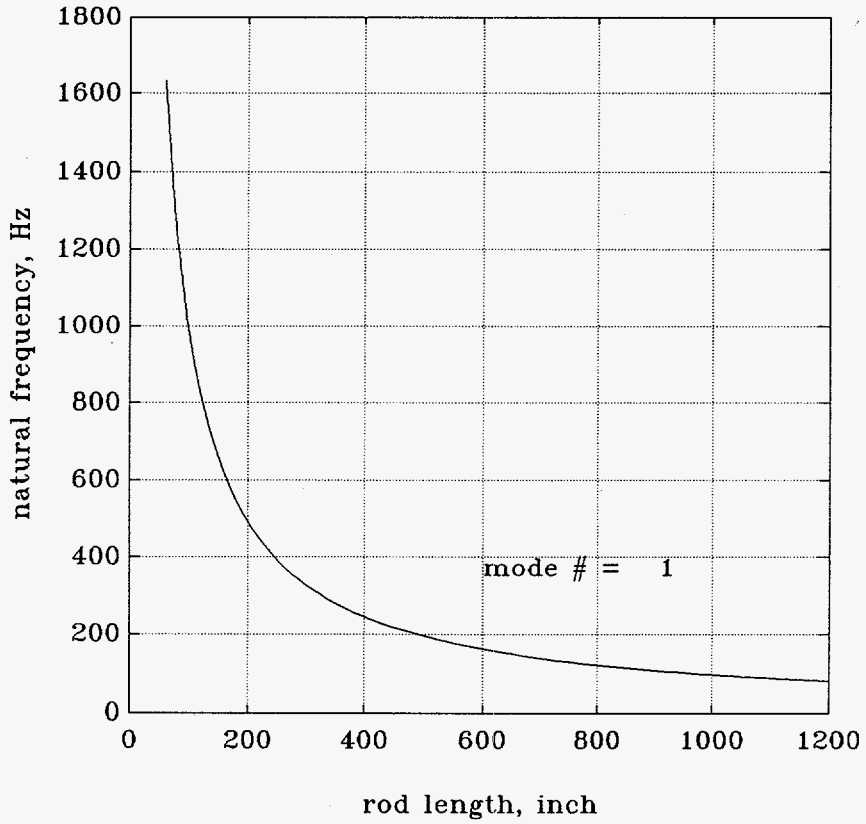

Figure 29. Natural frequency variation of the lowest mode versus rod length.

The equations presented in this section assume a rod free at both ends. In addition, the effects of damping were not considered. Under field conditions, the assumption of free end points does not apply strictly because the penetrometer tip is partially constrained by the soil. Therefore, the theoretical results presented serve only as a guideline for system selection. During penetrometer operations, the operator has to adjust the speed of vibrations according to the conditions encountered in the field in order to achieve an optimum penetration rate.

7.0 EXPERIMENTAL EVALUATION OF COMPONENTS

The main components of the steerable vibratory penetrometer system include the steerable tip, rod joints and their locks, and the POLO device and its umbilical. The performance of each of these components has to be verified before they are integrated into a full-scale system. In addition, the effects of vibrations on retarding forces of the soil and the effects of steering on the accuracy of POLO have to be determined.

In Sections 2, 4 and 5 the results of laboratory tests that aided in the design process were presented. In this section, the results of laboratory and field tests to verify component performance will be presented. The components to be tested include:

- steerable tip,
- locking joints,
- quick-connects, and
- POLO device.

The tests discussed in this section and Sections 2, 4 and 5 were re-run for repeatability whenever unexpected results were observed.

7.1 Steerable Tip Tests

Upon manufacture of the semi-passive steerable tip described in Section 2, the tip was attached to a field POLO unit and two sets of field tests were performed. The tests were carried out at Ft. Belvoir, and Fredericksburg, Virginia using the META-DRILL. The site soil at Ft. Belvoir consisted of very stiff clay, whereas the Fredericksburg site consisted of medium dense sand. The first objective of theses tests was to verify that the steerable tip changes from a symmetric position to an asymmetric position upon a 180° rotation of the rods from the surface. The second objective was to determine the radius of curvature of the bends generated by the steerable tip in different formations.

The tests started by setting up the META-DRILL at each site and connecting the POLO unit equipped with the steerable tip to the drill as shown in Figure 30. Initially the steerable tip was positioned in a symmetric position (for straight pushes). After six inches of penetration the drilling operation was stopped and the POLO unit was turned 180° counterclockwise. This was done to turn the steerable tip to its asymmetric position (for curved pushes). The POLO tracking program was then turned on and penetrometer operation resumed. The tests were completed after 74 inches of penetration in stiff clay and 173 inches in medium dense sand.

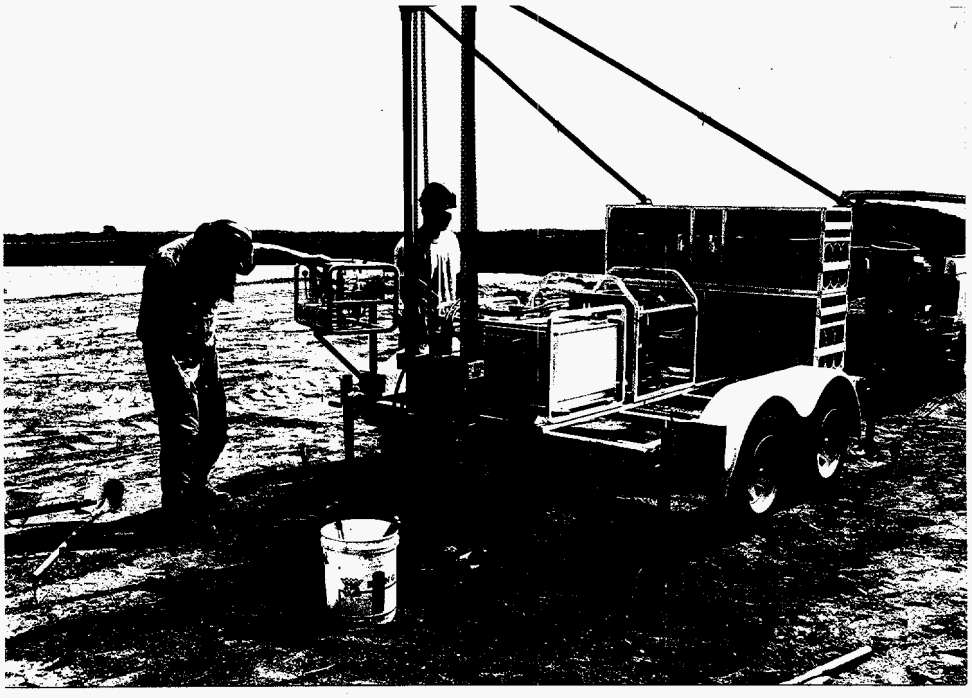

Figure 30. Steerable test set-up.

Table 1 shows the radius of curvature of penetrometer rods due to steering in each of the two sites. The radius of curvature for each test was obtained by using the POLO predicted coordinates of the tip. According to Table 1 the radius of curvature obtained in stiff clay was 114 ft, whereas that obtained in sand was 90 ft. It is worth noting that the initial inclination of POLO was vertical and all the tip displacements were due to bending of the rods by the steerable tip.

In Section 4 it was shown that off-the-shelf penetrometer rods are damaged at a radius of 85 feet. As a result the 114 and 90 foot radii of curvature generated by the steerable tip should not damage off-the-shelf rods as long as the curvature does not cause J hooking failure of the rods. J hooking failure occurs when the penetrometer rods as they go around a tight radius erode the confining soil around them.

Table 1. Steerable tip field test results.

Soil Formation	Radius of Curvature
Stiff Clay	114 ft
Medium Dense Sand	90 ft

7.2 Locking Joint Tests

In addition to bending tests of Section 4.1, laboratory and field performance tests were performed on the locking joints. The design torque for the locking joint had been selected at 9,000 in-lbs. The torque test was performed at 9,130 in-lbs without any damage to the locking joint mechanism. Figure 31 shows the torque test set up which consisted of 166 lbs of weights suspended from the end of a pipe wrench at 55 inches from the joint.

The field test carried out on the locking joint consisted of vibratory testing using the META-DRILL. Figure 32 shows the locking joint as assembled in the field. The purpose of this test was to push the locking joint into the ground and to examine its performance under the harsh vibratory environment. After several minutes of vibrations into the ground the locking joint was brought to the surface and examined. The examination indicated that with the exception of the shear plate ring that had come loose the entire assembly had remained intact and performed as expected. Based on this field test, a new shear plate with a positive lock was designed and manufactured.

Figure 31. Laboratory torque test set-up.

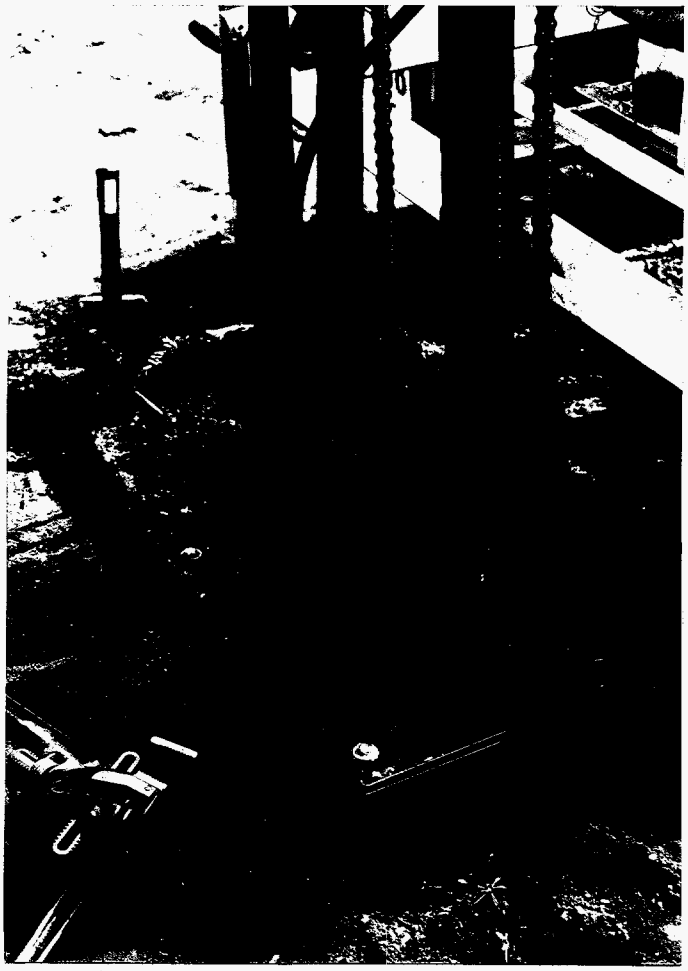

Figure 32. Field test on the locking joint.

7.3 Quick-Connect Tests

A quick connect for POLO umbilical was tested using the META-DRILL to determine the effects of vibrations on integrity of its components. The results showed no damage to the quick connect components and electrical contacts.

7.4 POLO Device Tests

POLO is one of the key components in the steerable penetrometer system. As a result it is essential to determine if it performs in a satisfactory manner under vibratory loading. During the field tests performed on the steering tip, POLO performed without any problems. The strain gage bridges were zeroed before each test and remained zero after each test. This implies that vibrations did not damage the gages and did not throw the bridges out of balance. The total time

when POLO was under constant vibration was approximately 90 minutes and the frequency of vibrations was in the 130 - 150 Hz range. This translates to an average of 750,000 cycles of vibrations.

7.5 Tests For Effects Of Vibrations On Retarding Forces

In normal penetrometer applications the retarding forces exerted by the soil on penetrometer rods depend on the geometry of the rods, and the type of soil. However, under vibratory loading the constant motion between penetrometer rods and the soil reduces the magnitude of the retarding forces because a dynamic rather than a static coefficient of friction applies, which in turn increases depth of penetration for comparable thrust levels. To test this hypothesis, two sets of field tests were carried out with the META-DRILL, at the sites where the steering tip was tested. The sites consisted of very stiff clay and medium dense sand.

In these tests, first the hydraulic thrusters of META-DRILL alone were used to thrust penetrometer rods into the ground. The vibratory drive was off during this stage of the test. The length of rods pushed into the ground was 32.5" in clay and 24" in sand under a thrust of 1500 lbs. After the rods stopped under the 1500 lbs of thrust, the vibratory drive was turned on, which made it possible to push additional lengths of rod into the ground equal to 53" in clay and 276" in sand.

The frequency of vibrations in clay was on the order of 100 Hz which translated to 1875 lbs of dynamic load. In sand the frequency of vibrations was 140 Hz which translated to 3,675 lbs of dynamic load. A quick review of the test results indicated that when the vibrations were turned on, the total thrust force was increased by 125% in clay, but the length of rods pushed increased by 163%. This is an indication that the dynamic nature of the load affected the soil-rod interaction. In sand the effects of vibrations were more pronounced, because by increasing the total force from 1,500 lbs to 5,175 lbs (1,500 lbs static + 3,675 lbs dynamic) or an increase of 245%, the length of rods pushed into the ground increased by 1,150%.

The effects of vibrations can be quantified in more detail by applying the principles of soil mechanics. When a rod is pushed into saturated clay (typical of the site soil), the thrust needed to overcome soil resistance is equal to:

$$F = pL\alpha c + cN_cA_p \qquad (16)$$

where F = thrust on top of the rod,
p = rod perimeter,
L = rod length,
α = adhesion factor,
c = soil cohesion,
N_c = cohesion factor,
A_p = cross-sectional area of the tip of the rod.

In a very stiff clay using a cohesion of 18 psi, an $N_c = 9$ (saturated clay), and the geometry of the penetrometer rods, it is possible to relate the length of rod pushed into the ground to the thrust force, if one knows the adhesion factor α. This is a factor that determines how much of the clay cohesion or stickiness is transmitted to the rod, which acts as a retarding force. For very stiff clay of the site, according to reference [4], α should be on the order of 0.4. To verify this number, α was calculated from Equation 16 using the test results obtained under hydraulic thrust conditions alone. The following numbers were substituted in the equation: F = 1,500 lbs, L = 32.5, $A_p = 2.4$ in^2, c = 18 psi, and $N_c = 9$. This resulted in $\alpha = 0.42$.

For stiff clay of the site Equation 16 was used a second time using the parameters measured during the vibratory phase of the field test. The following numbers were substituted in the equation: F = 3,375 lbs, L = 85.5", $A_p = 2.4$ in^2, c = 18 psi, and $N_c = 9$ which resulted to $\alpha = 0.38$. This is a 10% improvement (reduction) over the number obtained under hydraulic thrusting alone. The reduction is encouraging considering the very stiff condition of the clay at the site, which inhibited relative motion under vibratory conditions. In a less stiff clay the reduction in the adhesion factor is predicted to be larger.

To quantify the effects of vibrations in sand the following equation was used for thrust as a function of rod length:

$$F = \Sigma p \Delta L f + A_p q N_q \qquad (17)$$

where F = thrust on top of the rod,
Σ = summation over rod length,
p = rod perimeter,
ΔL = segmental rod length,
f = skin resistance factor,
A_p = cross-sectional area of the tip of the rod,
q = effective vertical stress at pile depth or at a limiting depth,
N_q = point resistance factor.

The equation for the skin resistance factor, f is:

$$f = K \sigma_v \tan\delta \qquad (18)$$

where K = passive earth pressure coefficient = $\tan^2(45+\phi/2)$,
ϕ = angle of internal friction of sand,
σ_v = average vertical effective stress over segment length, ΔL, and
$\tan\delta$ = coefficient of friction between sand and rod.

In a medium dense sand the static properties are $\phi = 40^0$, $\tan \delta = 0.5$ and $N_q = 300$. Using these properties along with a unit weight of 120 pcf (to calculate q and σ_v) the required thrust for 300 inches of rod is 10,052 lbs. However, during the vibratory field tests a total of 5,175 lbs of static plus dynamic force was necessary to push penetrometer rods 300" into the ground. This shows a 48% reduction in retarding forces due to the effects of vibrations on the coefficient of friction, $\tan \delta$, and the coefficient of earth pressure, K.

8.0 POLO INTEGRATION INTO A SCAPS TRUCK

Capabilities of the prototype POLO system were demonstrated under a DOE sponsored PRDA contract in July, 1994. The optimum way to make commercial POLO systems available to DOE contractors was to develop a commercial system and integrate it into a SCAPS truck. This effort involved the design and manufacture of a commercial POLO module and initializer, and integration of a user friendly data acquisition package into the POLO system.

After manufacturing and assembly of the commercial POLO components, field tests were conducted to demonstrate the capabilities of the commercial system. Details of these tests are presented in Section 9.

8.1 Commercial POLO And Initializer

Based on lessons learned during the prototype POLO field tests of July, 1994 and the study of the system presented in Section 5, it was decided to use a similar design for the commercial POLO module body and strain gaging as shown in Sections 5.1 and 5.2. This will enable the penetrometer operator to use the same POLO system in both straight ahead and steerable modes.

In addition to the POLO module body, another component of POLO that was redesigned for commercial purposes was the POLO initializer. The new commercial initializer is shown in Figure 33. This is an electronic/mechanical device that is used to measure the initial angles of the penetrometer rod as it begins to penetrate the soil surface. This device has an aluminum frame and moving parts made of steel. It has two electronic angle sensors called clinometers which connect by wire to a computer in the penetrometer truck.

There are three angles that completely describe the global orientation of the POLO rod: the elevation, azimuth and rotation angles as shown in Figure 34. The elevation angle is the angle between a vertical line and the longitudinal axis of the POLO rod. The azimuth angle is the angle between a plane which includes the two lines just described and a plane which includes a vertical and a northerly line. The rotation angle describes the orientation of the reference strain gage with respect to the plane containing the elevation angle.

When the initializer is attached to the POLO module, the two initializer clinometers read the elevation angles of two orthogonal axes perpendicular to the longitudinal axis of POLO. Using these two angles and trigonometric relations, the elevation, and azimuth angles of POLO are calculated by the POLO program.

In addition to providing the elevation and azimuth angles, the initializer can be used to load the POLO module along a predetermined bend plane by turning the hand wheel on the initializer. Once the POLO module is loaded, the POLO program automatically calculates the location of the reference gage on the module body with respect to the predetermined bend plane and calculates the rotation angle accordingly.

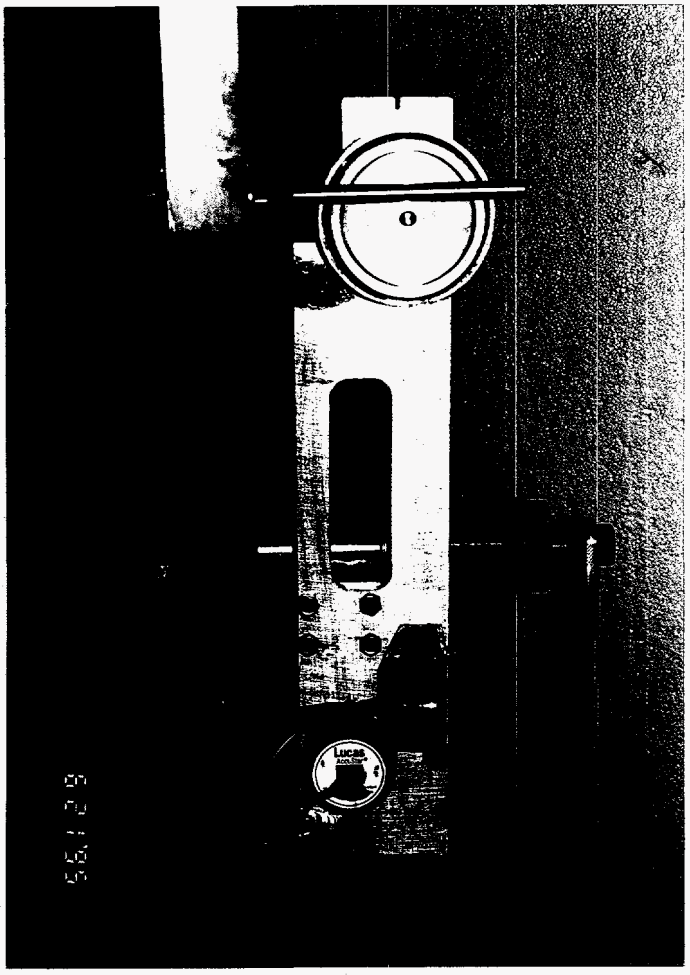

Figure 33. Commercial POLO initializer.

8.2 Commercial POLO Data Acquisition Package

One of the critical tasks in the operation of the POLO system is gathering of strain gage data and transmission to the surface computer for further processing. Two types of data acquisition (DAQ) packages can be used for this purpose. One type deals with all of the data processing hardware on the surface and the second type deals with miniaturized data processing hardware that fits inside the POLO module for down-hole processing.

A surface type portable DAQ system was used in field testing and demonstration of the prototype POLO system in July, 1994. With this setup the wires from all the strain gage bridges were extended to the surface. The umbilical making up the 24 wires had to be pre-threaded through the rods that were intended to be pushed into the ground. Because of the thickness of the umbilical, the pre-threading process was time consuming and there were instances where the

umbilical was severed by field workers. Another problem associated with surface type DAQ systems is susceptibility of the strain gage signals to noise. Strain gage signals are analog signals which attenuate over long distances and can pick up noise on their way to the surface.

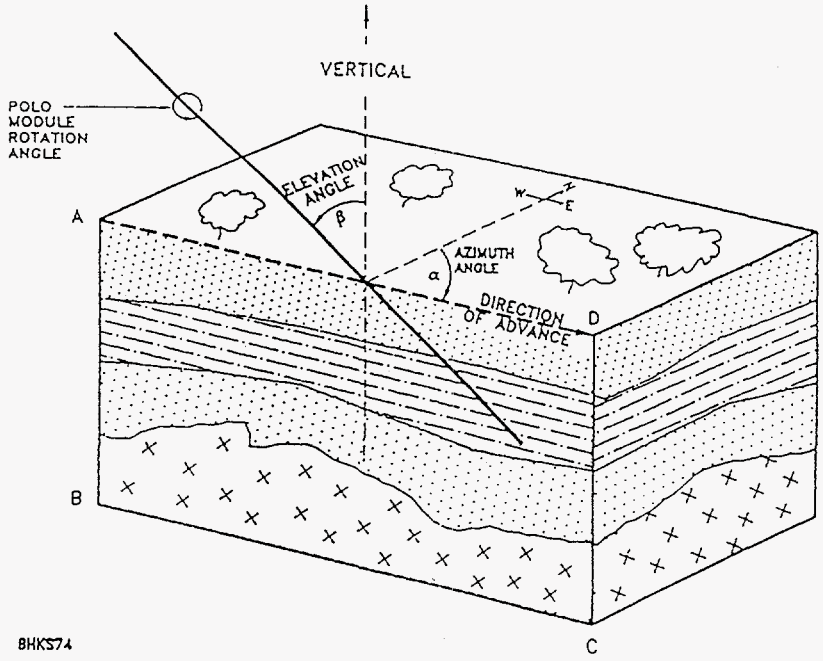

Figure 34. Initial angles of POLO.

Realizing the problems associated with surface type DAQ systems, UTD undertook an internal research and development program to develop a down-hole DAQ system. With this system all the signal conditioning and processing occurs inside the POLO module, and a digitized signal is sent to the surface computer with two wires. The same two wires are used for powering strain gages and the DAQ system. The two-wire umbilical is much easier to handle in the field than a 24-wire umbilical, and occupies less space inside the penetrometer rods. Other advantages of a down-hole DAQ system are that the analog signal travels a short distance before it is digitized, thereby greatly reducing the potential for noise pickup, and the digital signal that travels to the surface computer assures an error free acquisition. More details regarding the UTD down-hole system were presented in Section 5.3 and Figure 24.

9.0 POLO FIELD TESTS

Two sets of field tests were performed for performance demonstration of the commercial POLO system. During the first set of field tests POLO was inserted into the ground in a sub-horizontal mode. The purpose of these tests was to survey the penetrometer tip as it daylighted inside an excavated pit. Upon successful completion of the sub-horizontal tests, field trials were made with POLO using DOE's SCAPS penetrometer truck. The purpose of these trials was to familiarize the SCAPS truck operator with the use of POLO, debug the system and ensure that the commercial POLO system fits within the constraints of the SCAPS truck.

9.1 Sub-horizontal field tests

The sub-horizontal field tests on POLO were performed in Atlanta, Georgia using a rod pusher provided by Ditch Witch of Georgia. Figure 35 shows the test setup and the rod pusher. Field tests were performed with POLO penetrating the ground at shallow angles (less than 10 degrees from horizontal) towards a pit excavated some distance from the point of insertion. The objective of these tests was to push rods into the ground until the penetrometer tip and POLO daylighted inside the excavated pit. Standard surveying techniques were used to survey the exit hole inside the pit and the results were compared with POLO predicted coordinates. Figure 36 shows the surveying in progress.

Four successful tests were completed in Atlanta. A test was deemed successful if the penetrometer tip exited inside the excavated pit. In some instances boulders or cobbles blocked the advance of the rod pusher and in some other instances the penetrometer tip surfaced out only after 5 to 10 feet of advance. The results of the four successful sub-horizontal tests are presented in Table 2.

In Table 2 the first column indicates the test number. In test number 2 two exit pits were excavated and the exit hole in each pit was surveyed. The second column in the table shows the total shove length for each test. Shove lengths varied from 378 inches (31 ft) to 743 inches (62 ft). The X, Y, and Z under the POLO heading are those predicted by POLO, whereas those under the survey heading were obtained by standard surveying methods. The % Error column is % error as a function of distance traveled (shove length) and is calculated as:

$$e = \frac{\sqrt{(X_P - X_S)^2 + (Y_P - Y_S)^2 - (Z_P - Z_S)^2}}{\text{shove}} \times 100\% \qquad (19)$$

where e = % Error
X_P, Y_P, Z_P = X, Y, Z coordinates predicted by POLO,
X_S, Y_S, Z_S = surveyed X, Y, Z coordinates.

Figure 35. Sub-horizontal field test set-up.

The % error column in Table 2 indicates that POLO accuracy ranged from 0.16% to 0.52%. An independent check of the surveying method indicated that the surveyed coordinates can be off by +/-1 inch. Taking this into account for tests number 2a and 2b the POLO error for all the tests falls below 0.50%.

9.2 SCAPS truck field tests

At the conclusion of sub-horizontal field tests, the POLO system was mobilized to a site local to Applied Research Associates (ARA) Incorporated in South Royalton, Vermont in order to test POLO within the confines of a SCAPS truck and to familiarize the SCAPS operator with the use of POLO. Figure 37 shows the POLO computer inside the SCAPS truck operator compartment. In Figure 38, POLO initialization is in process. Table 3 shows the results of two field tests carried out with the SCAPS truck. In test No.1 a standard conical penetrometer tip was used. However, due to an underground obstacle (either an inclined hard layer, or a cobble) the path deviated from straight line and ended at about 62 inches off center at a depth of 617 inches.

Figure 36. Sub-horizontal test survey.

In test No. 2, an angled wedge was used at the tip of the penetrometer instead of a conical tip. At the moment of insertion into the ground the tip wedge was oriented in such a way that the unbalanced forces acting on the tip would force the tip in the +X direction. As shown in Table 3, it is observed that as expected the tip deviated in the -X direction by only 7.0 inches instead of 61.5 inches.

The SCAPS truck field tests were deemed successful because the operation of POLO did not interfere with normal operations of the truck and indeed as the test results indicate POLO successfully predicted the expected path of a wedge tipped penetrometer.

Table 2. Sub-horizontal test results.

Test No.	Shove Length (in.)	POLO			SURVEY			Error (%)
		X (in.)	Y (in.)	Z (in.)	X (in.)	Y (in.)	Z (in.)	
1	489.8	-13.1	484.6	-69.0	-12.5	484.4	68.6	0.16
2a	479.3	-10.2	478.2	-24.5	-9.5	478.3	-26.9	0.52 (0.29)
2b	743.4	-18.9	741.8	-36.3	-20.4	742.1	-32.8	0.51 (0.35)
3	378.2	17.6	369.5	-80.6	16.9	369.8	-79.4	0.38
4	524.2	-6.3	518.8	-74.3	-6.3	518.4	-72.6	0.33

( ) = taking into account +/- 1 in. error in surveyed coordinates.

Table 3. SCAPS truck test results.

Test No.	Shove Length (in.)	POLO		
		X (in.)	Y (in.)	Z (in.)
1	621.0	-61.5	2.1	-616.9
2	394.0	-7.0	-1.2	-393.9

Figure 37. POLO computer in SCAPS truck.

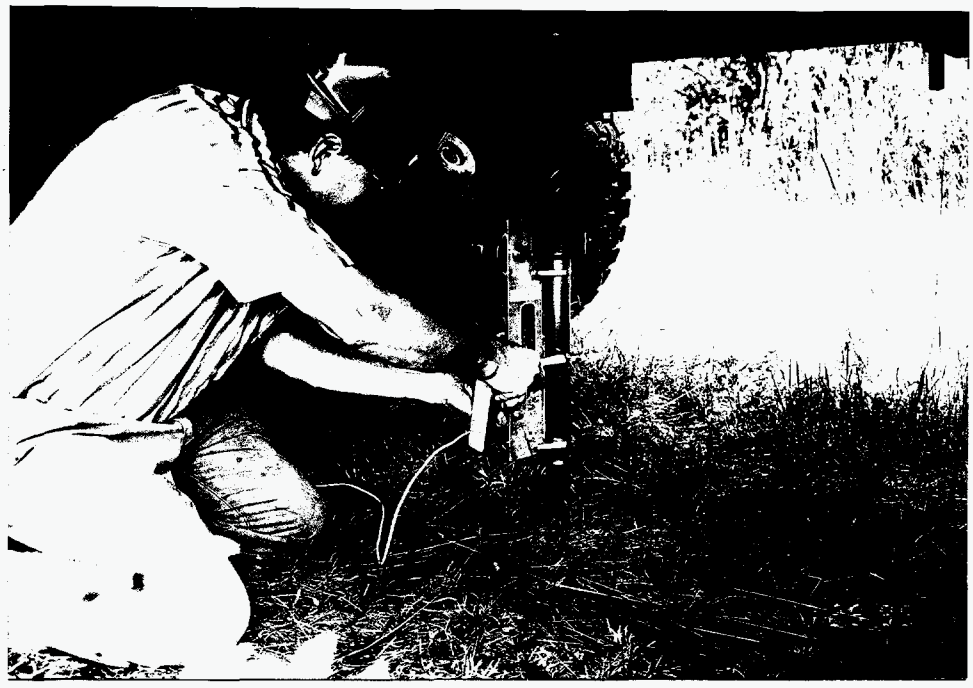

Figure 38. POLO initialization in progress.

10.0 CONCLUSIONS AND RECOMMENDATIONS

10.1 Conclusions

The progress reported in this report covers three technology areas that will lead to an enhanced system and new market areas for penetrometers. The three technology areas are steerability, vibratory penetration, and real-time tracking of the penetrometer.

In the area of steerability, the results of sub-scale analysis, design, and laboratory and field tests indicated that controlled steering of penetrometers is feasible. To accomplish this it is necessary to have a steerable penetrometer tip and penetrometer joints that can withstand bending moments due to curved steering. In addition, the joints have to be locking to resist steering torques. Finally, the key to steerable penetration is POLO which allows the operator to know the location of the penetrometer tip at the end of each push cycle.

The results regarding vibratory penetration indicated that vibrations enhance the penetration depth by reducing the magnitude of retarding forces. It was shown that vibrations in very stiff clay reduced the adhesion factor by 10%. This reduction is expected to be higher in softer clays. In medium dense sand the retarding force was reduced by 48%.

The effort regarding the integration of a commercial POLO system into a SCAPS truck resulted in a reconfigured module body and more user friendly initializer and tracking software. Field tests on the commercial POLO indicated that errors of less than 0.50% were achievable with POLO. They also indicated that POLO can be operated within the confines of a penetrometer truck without hindering the normal operations of the truck.

Specific results of each task were as follows:

Task 1.1 Environmental Work

Uncontaminated sites were selected in Virginia for Phase 1 field tests.

Task 1.2 Steerable Wedge Design

An analytic model for performance of steerable wedges was developed and verified by comparison with laboratory test results on simulated steerable penetrometer rods. This effort led to manufacture of a prototype steerable tip.

Task 1.3 Survey of Vibratory drives

A vibratory drive unit was purchased for the purpose of Phase 1 limited field tests and Phase 3 full-scale field tests.

Task 1.4 Joint Design

A new joint was designed for steerable penetrometer rods. In addition, a locking mechanism was designed to keep the joint locked under steering torques. Laboratory tests verified superior performance of the locking joints both in strength relative to conventional joints and in the ability of the lock to prevent loosening of the joint.

Task 1.5 Design of POLO Umbilical

A set of quick connects were designed to carry POLO signals to the surface computer using penetrometer rods as one conductor and a wire internal to each rod as the other. This configuration is used with UTD's downhole data acquisition package which conditions strain gage signals of POLO and sends a multiplexed digital signal to the surface computer using two conductors.

Task 1.6 POLO Adaptation

The original POLO design was modified to make the downhole unit survivable under the more rugged conditions expected during vibratory penetration.

Task 1.7 Theoretical Systems Analysis

A theoretical analysis was performed to determine the effects of vibrations on system components. The results were used to determine bounds or operational requirements of the vibratory components.

Task 1.8 Experimental Evaluation of Components

Laboratory and field tests were performed to evaluate component performance and to generate data for design purposes. The results indicated that each major component satisfied its design requirements.

Task 1.9 Design of Commercial POLO unit

A commercial POLO system was designed and manufactured with user friendly components and a tracking program.

Task 1.10 Data Acquisition Integration

UTD's downhole data acquisition system was integrated with a commercial POLO rod. The system uses less than 20% of the inner area of the rod, leaving the rest for other umbilicals to pass through.

Task 1.11 Calibration and Field Tests

A user friendly calibration frame was designed and manufactured for POLO rods. The commercial POLO rod was calibrated and sub-horizontal field tests were performed to determine system accuracy. Test results indicated that accuracies of better than 0.5% of distance traveled are achievable with the POLO system. After sub-horizontal tests, the POLO system was tested in DOE's SCAPS truck and the truck operator was trained in the use of POLO.

10.2 Recommendations

The contract for the steerable/distance enhanced penetrometer delivery system is comprised of a base year program (Phase I) for sub-scale major subsystems analysis and design, and two optional phases (Phases II and III) for full-scale systems design integration and testing. The results presented in this report are for the base year program (August, 1994 - August, 1995) and they indicate that the full development of a steerable/distance enhanced penetrometer delivery system is indeed feasible. As a result, UTD, Incorporated recommends continuation of the development effort with start work on Phase II as scheduled.

11.0 REFERENCES

[1] Das, B.M., PRINCIPLES OF FOUNDATION ENGINEERING", 2nd edition, PWS-KENT Publishing Company, Boston, 1990.

[2] Winterkorn, H.F., and Fang, H-Y, FOUNDATION ENGINEERING HANDBOOK, Van Nostrand Reinhold Company, New York, 1975.

[3] Meirovitch, L., ANALYTICAL METHODS IN VIBRATIONS, The MacMillan Company, London, 1967.

[4] Bowles, J.E., FOUNDATION ANALYSIS AND DESIGN, 2nd edition, McGraw-Hill Inc., 1977.

APPENDIX A

TEST PLAN FOR LABORATORY STEERING TESTS

A.1 TEST APPARATUS AND PROCEDURE

The test apparatus comprises of a 4'x1'x5' sandbox with a transparent acrylic window as its front panel, as shown in Figure A-1. The window was supported at its center by a transverse beam to prevent excess deformation under the soil pressure.

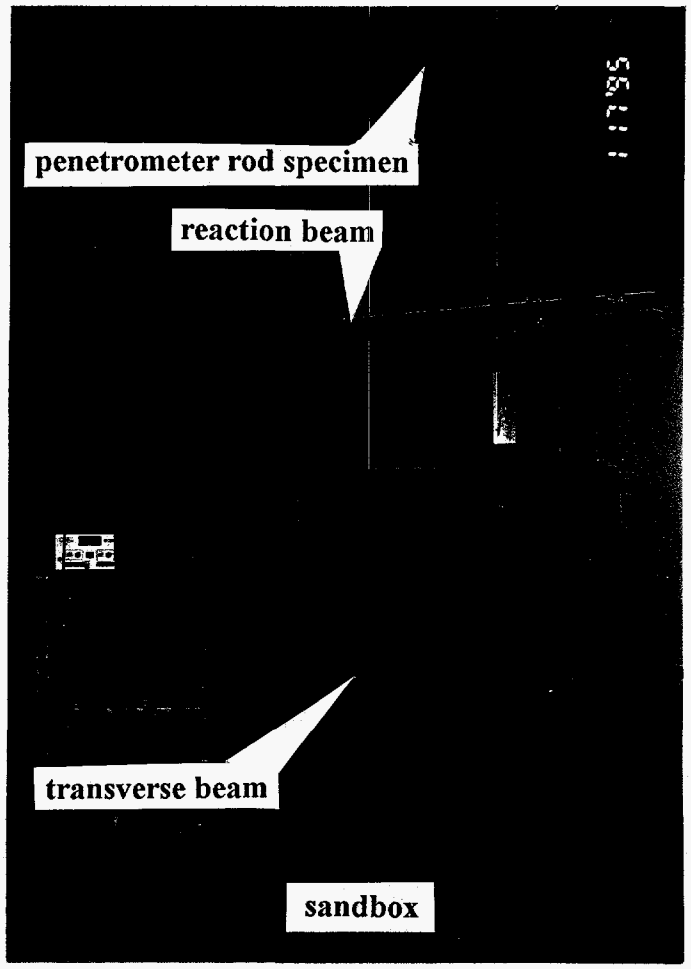

Figure A-1. The sandbox test apparatus.

The lines seen on the front window form a mesh of 5"x5" grid boxes. Two brackets are attached to the side walls supporting a steel reaction-beam. A grip-box guide mounted on top of the sandbox frame, as depicted in Figure A-2, supports a rod grip-box permitting only its vertical degree of freedom. A two-ton hydraulic jack mounted between the rod grip-box and the reaction beam is capable of generating thrust to force the grip-box down toward the sand. A load cell mounted between the jack and the reaction beam, as shown in Figure A-3, records the thrust load on-line. The grip-box design is based on a mechanical wedge principle where friction is utilized to provide a unidirectional latch mechanism, as depicted in Figure A-4.

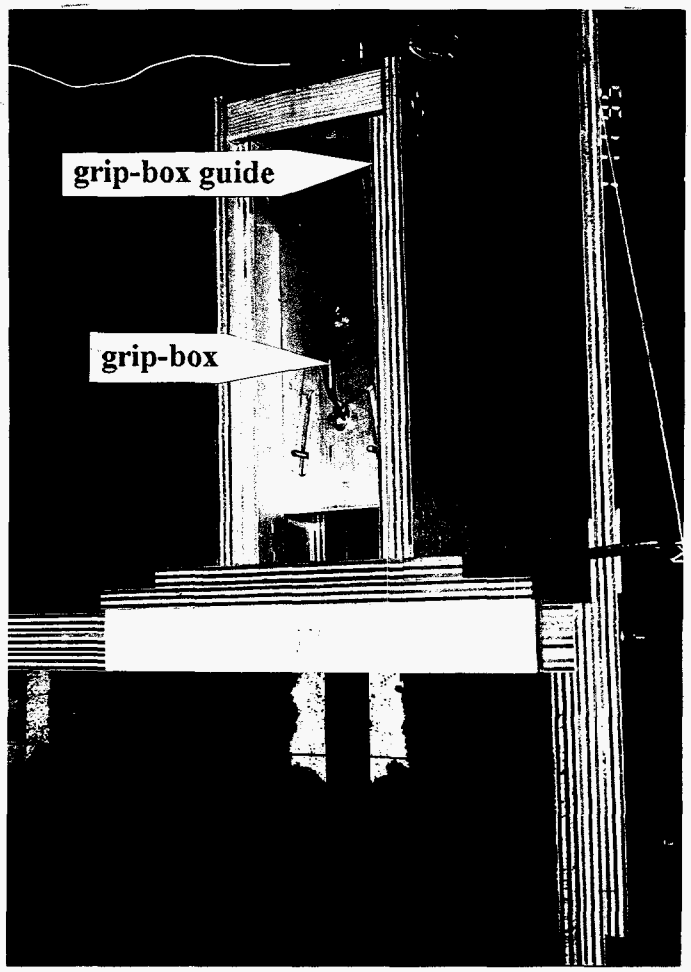

Figure A-2. Rod grip-box and guide.

The soil used for the experiment was a commercial-grade all purpose sand. Using this apparatus, a test is conducted by pushing a rod specimen into the soil. The stiffness of such a rod has been significantly reduced so as to allow observable deformations. The rod is lifted up and then inserted into the grip-box between the two wedges all the way down to the soil top surface. Sliding the grip-box up, the wedges are locked on the ready-to-push rod. Activation of the hydraulic jack for strokes of about two inches long each, causes the rod to penetrate the soil. Load measurement is recorded on-line and tip position coordinates are evaluated and recorded at the end of each stroke. Two different sets of tests were conducted. The first set was two-dimensional steering tests which provided insight to the steerability characteristics, and the second set was three-dimensional steering tests which provided first-hand application of a real-time field test in a laboratory environment.

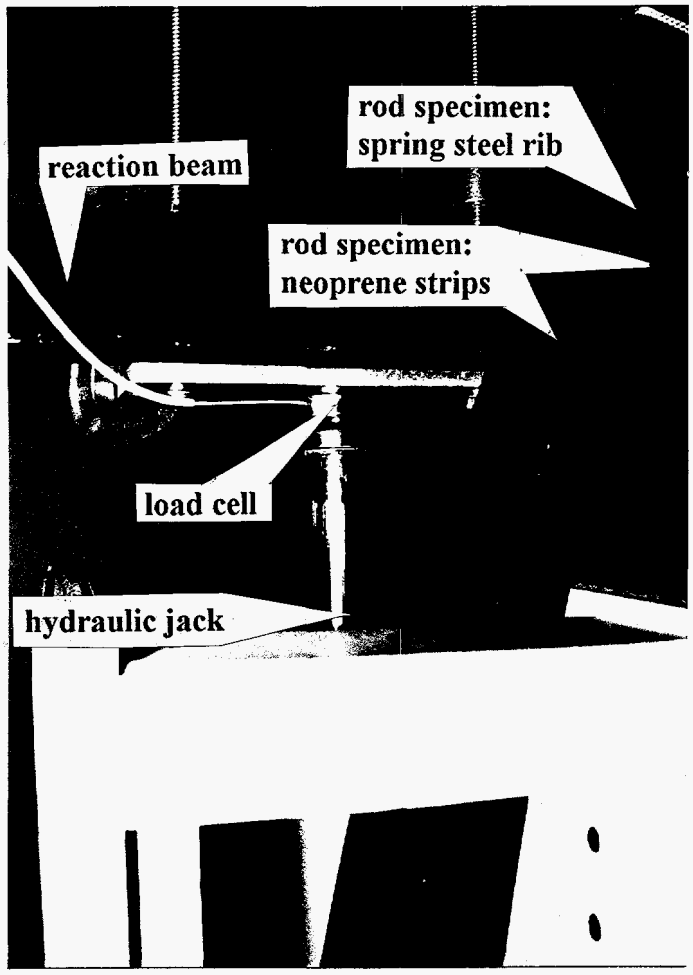

Figure A-3. Force generation and force measurement system.

A.2 THE TWO-DIMENSIONAL TEST SETUP AND PROCEDURE

The two-dimensional (2-D) test setup is a technique for evaluating and quantifying the directional tip steering capabilities. The rod specimen is comprised of two rectangular cross-sectional, eight feet long, neoprene bonded onto both sides of a spring-steel rib, as depicted in Figure A-3. The tips on both sides of the rod were cut to reflect 5° and 10° wedges, reinforced by steel plates, one of which may be seen in Figure A-4. The essential characteristics of the 2-D rod is in its bending stiffness properties. While possessing a significantly "low stiffness" about one of the bending axes, "rigid"characteristics prevent bending about the other. For the 2-D test, the back wall of the sandbox was assembled close to the front window so as to confine the rod to an in-plane motion only. The gap between the two panels was filled with compacted wet sand. The main feature of this setup was in the ability to observe the development of the rod trajectory as it was pushed into the soil.

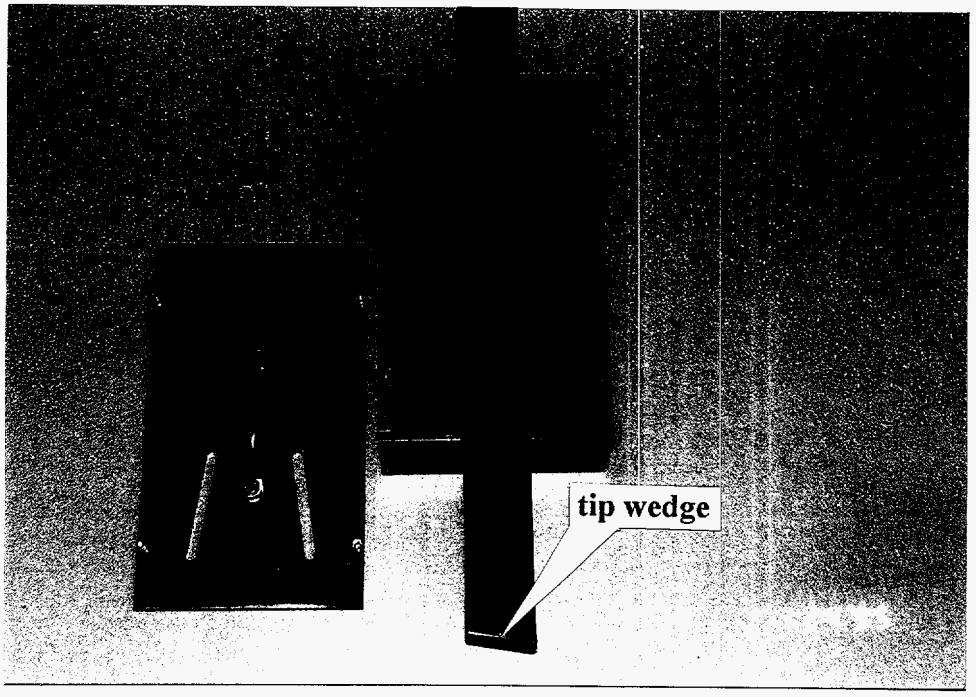

Figure A-4. Grip-box latch mechanism.

Experiment Parameters:

Soil

soil density	120 lb/ft^3
angle of soil internal friction	35°
angle of soil-rubber surface friction	28°
bearing capacity parameter	170

Rod:

rubber cross-sectional dimensions	1.50x0.75 in
steel cross-sectional dimensions	0.75x0.0625 in
bending stiffness EI (experimental)	598 lb-in^2

A.3 THE THREE-DIMENSIONAL TEST SETUP AND PROCEDURE

The three-dimensional (3-D) test setup is the ultimate testing method that provides first-hand application of a real-time field test in a laboratory environment. The method permits directional penetration with steerability enhancement using a directional tip in the form of a wedge or an oblique cone, as depicted in Figure A-5. The rod specimen is comprised of an eight feet long cotton-braided neoprene hose, reinforced by a piano wire core that passes tight through the center-hole of cylindrical wooden beads. Any two of the beads in this arrangement were kept apart by a loosened-center spherical spacer, as shown. Changing of the spacer's diameter permits the modulation of overall stiffness of the rod specimen. Two tip configurations were tested, one in the form of a

rounded directional wedge, and the other in the form of an oblique cone. Figure A-5 displays a 5° rounded wedge tip and two 40 ° cones, with their cone center-line tilted, one at 5 ° and the other at 10 °.

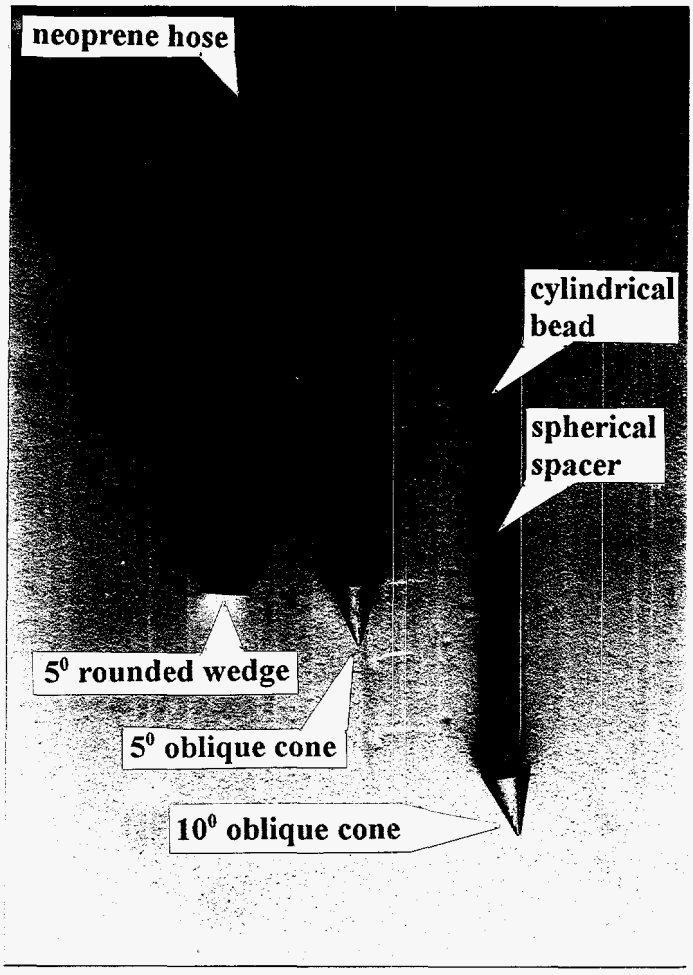

Figure A-5. 3-D rod specimens with directional tip.

For the 3-D test, the back wall of the box was assembled at its most remote position from the front window and the entire box was filled with dry sand. The main feature of this setup was the ability to push the rod in an arbitrary direction and to monitor the penetration load of a field-test-like rod. Unable to observe the development of the rod penetration trajectory inside the soil, the front window was selected as the final destination where the tip position at the terminal point could be located.

Experiment Parameters:

Soil

soil density	120 lb/ft^3
angle of soil internal friction	38°
angle of soil-rubber surface friction	28°
bearing capacity parameter	250

Rod:

rubber hose cross-sectional dimensions	1.25x0.75 in, outer-inner diameters
piano wire cross-sectional dimensions	0.125 in, diameter
bending stiffness EI (experimental)	896 $lb\text{-}in^2$